Deliverable D 1.3

Characterization of the railway environment: channel models & general characteristics

Project acronym:	EMULRADIO4RAIL
Starting date:	01/12/2018
Duration (in months):	18
Call (part) identifier:	H2020-S2R-OC-IP2-2018-03
Grant agreement no:	826152
Due date of deliverable:	Month 12
Actual submission date:	31/07/2020
Responsible/Author:	Juan Moreno - MdM
Dissemination level:	PU
Status:	Draft

Reviewed: (yes)

Document history		
Revision	Date	Description
01	01/12/2019	First issue
02	31/07/2020	Inclusion of new TDL channel models for tunnels
03	21/12/2020	Changes requested by reviewer and inclusion of a new reference for a recently accepted paper

Report contributors		
Name	Benificiary Short Name	Details of contribution
Juan Moreno	MdM	Contribution on the railway channel choices and global review. Changes in overleaf for both 2nd and 3rd version
Romain Behaegel	Ifsttar	Contributions on general state of art for channel models and railway channel models, help on layout on overleaf
Marion Berbineau	Ifsttar	Contributions on general state of art for channel models and railway channel models and general review
Yann Cocheril	Ifsttar	Help on Layout on overleaf
Laurent Clavier	Univ. Lille	General final review

Contents

List of Figures

List of Tables

1 Executive Summary

To avoid a complicated validation process with costly on-site testing for new Train-to-Ground (T2G) communication systems, the European EMULRADIO4RAIL Project will provide an innovative emulation platform for tests and validation of various radio access technologies (RAT) like Wi-Fi, GSM-R, LTE, LTE-A, 5G and Satcoms. The emulation platform will combine simulations of the communication core network and emulation of various RATs thanks to the coupling of discrete event simulator such as RIVERBED Modeler, Open Air Interface, several radio channel emulators, models of IP parameters and real physical systems.

The number of RATs to be considered has been aligned with the X2RAIL-3 WP3 prototypes. Mainly four RATs are considered: Wi-Fi, 3GPP LTE, 5G NR and Satellite communications. Satellite systems are emulated at IP levels. Consequently, they are not considered in this report. We attract the attention that as explained in D2.1 [18], 5G NR is not considered due to the fact that 5G NR features are not available for the Open Air Interface platform at the moment of writing this Deliverable.

This deliverable intends to provide a complete description of following topics:

- A complete description of the radio channel models to give a solid basis to understand the State of Art,
- An exhaustive state of the art made with a large literature survey on railway channel models
- The methodology followed to retrieve the radio channel models that are most suitable for the emulation platform.
- The description of the chosen models. This task had input from T1.1 (railway scenarios) and T1.2 (degraded situations) and has been an input for both T2.1 and T2.2.

2 Abbreviations and acronyms

5G	5th generation
AA	Adjacent Area
AoA	Angle of Arrival
BPSK	Binary Phase Shift Keying
BS	Base Station
CA	Close Area
CBTC	Communications-Based Train Control
CDL	Clustered-Delay Line
CIR	Channel Impulse Response
CRS	Cell Reference Signal
DA	Distant Area
EM	Electro Magnetic
ETCS	European Train Control System
FT	Fourier Transform
GBSCM	Geometry based stochastic channel model
GSM-R	GSM for Railways
HSL	High Speed Line
HST	Hight Speed Train
IEEE	Institute of Electrical and Electronics Engineers
IMT-A	International Mobile Telecommunications-Advanced
IP	Internet Protocol
ISI	Inster-Symbol Interference
ISM	Industrial, Scientific and Medical
ITU	International Telecommunication Union
LOS	Line-of-Sight
LTE	Long-Term Evolution
LTE-A	Long-Term Evolution Advanced
MIMO	Multiple-Input Multiple-Output
MRS	Moving Relay Stations
NGSCM	Nongeometric Stochastic Channel Model
NLOS	Non LOS
NR	New Radio
PDP	Power-Delay Profile
PL	Path-Loss
QoS	Quality of Service
RA	Remota Area
RATs	Radio Access Technologies
RMS	Root Mean Square
SCM	Spatial Channel Model
SCME	Spatial Channel Model Extended
SISO	Single-Input Single-Output
SV	Saleh-Valenzuela
T2G	Train-to-Ground
T2T	Train-to-Train
TDL	Tapped-Delay Line
UMTS	Universal Movile Telecommunication System
US	Uncorrelated Scatterers
WCDMA	Wideband Code Division Multiple Access
Wi-Fi	Wireless-Fidelity
WSS	Wide-Sense Stationary
WSSUS	Wide-Sense Stationary Uncorrelated Scatterers

3 Background

The present document constitutes the Deliverable D1.3 ”Characterization of the railway environment: channel models and general characteristics” in the framework of the EMULRADIO4RAIL project (GA 826152), WP1/Task 1.3. This Deliverable follows an internal document (Milestone 2), which included the preliminary cut of channel models and also some premises to start the discussion in order to agree on the criterion to choose the final ones.

This characterization will be considered as a basis to build channel models as well as other representative characteristics for the railway applications and scenarios considered in the emulation platform. Once the railway scenarios have been identified (see D1.1 [19] as well as the sources of perturbations to be considered (in the internal milestone 2, plus in D1.2 [20], it is needed to go to the literature in order to retrieve suitable channel models for all these physical layer aspects to be introduced in the platform.

4 Objectives

This document has been prepared to identify a set of suitable radio channel models for the different railway scenarios to be emulated in the Emulradio4Rail platform. These scenarios are: tunnel, rural, cuttings, viaducts and hilly. For each of them we reference all the channel models found in the literature, plus the information provided for each one of them (unfortunately, this information very often is not complete in terms of required knowledge such as Doppler, number of taps, *etc.*). Then, after a detailed literature survey, we introduce a methodology to pick up the most suitable railway models to be emulated in accordance with the technical potentialities of the channel emulators considered in the project. Finally, the final set of selected models is given.

Moreover, in order to provide some context for this deliverable, a section describing the most relevant topics on physical layer modelling (*i.e.* 'channel modelling') is included in this Deliverable as well. This deliverable provides a complete description of following topics:

- A complete description of the radio channel models to give a solid basis to understand the State of Art,
- An exhaustive state of the art made with a large literature survey on railway channel models
- The methodology followed to retrieve the radio channel models that are most suitable for the emulation platform.
- The description of the chosen models. This task had input from T1.1 (railway scenarios) and T1.2 (degraded situations) and has been an input for both T2.1 and T2.2.

5 Context

In this section both inputs for this task 1.3 are explained: railway scenarios (from T1.1, which was released in Deliverable D1.1 [19]) and the perturbations to be introduced in the platform (from T1.2 and Deliverable D1.2 [20], which will be released at the same time as this Deliverable).

5.1 Railway scenarios (input from T1.1)

The first task within this Project was focused on the definition of the application layer requirements for Communication systems in railway environments. Therefore, a description of both the different railway scenarios to be covered (high-speed, urban, regional, *etc.*) and the services (CBTC, video surveillance, ETCS, *etc.*) was provided. Moreover, some data traffic models for these communication services, IP-layer parameters, QoS definition and quality metrics were identified as well.

In terms of the impact on other tasks, the main outcome from task 1.1 was the identification of scenarios and services to be emulated in the platform. Regarding the scenarios with physical-layer impact, we decided to include the following:

- Tunnel
- Rural
- Cutting
- Viaducts
- Hilly

Obviously, tunnels are a vital scenario for subways and for mainline and high-speed but on a lesser extent. Cuttings and viaducts are essential in modern high-speed lines which tend to be built avoiding steep ramps and strong curves. Finally, both rural and hilly should be considered as basic scenarios on both main lines and high-speed lines.

It is important to note here that due to the fact that satellite bearer will be emulated only at IP level, this report will not detail satellite channel models.

5.2 Perturbations to be introduced (input from T1.2)

Potential sources of degradation of the radio links on railway scenarios and a quantification of their impact are analyzed in D1.2 report [20]. This includes EM interferences, network interferences (interference induced by other communication networks using the same or adjacent frequencies), non-intentional EM interference sources (the most significant being transient EM interferences produced by the catenary-pantograph contact loss) and intentional EM interferences (produced by jammers on board of the train or on the track side). These perturbations models will be added to the radio channel models in the channel emulators as described in [20], [18] and [21].

Once the detailed characterization of all of them and the study on their impact, a decision was made on which one of them were to be included in the emulation platform. Finally, we identified three perturbations:

- Network interference in the ISM band,
- Sliding contact between the pantograph and the catenary,
- Illegal jamming.

6 Mobile radio propagation generalities and modelling

6.1 Introduction

This chapter will present the main characteristics of the mobile radio channel. We will introduce the main parameters that allow to characterize the radio channel and that will be considered later for channel emulation. The last section is about multipath channel modelling. We will introduce the channel impulse response.

6.2 Main characteristics of the mobile radio channel

The mobile radio channel places fundamental limits on the performance of a mobile communication system. Compared to predictable and stationary wired channels, mobile radio channels are extremely random. This section explains the main phenomena that we will have to take into account in this work. The main references considered are [22],[23],[24].

6.2.1 Multipath

Following the optical analogy, the different obstacles between the transmitter and the receiver cause signal variations due to phenomena such as reflections, diffraction, scattering and diffusion as illustrated Figure 1. The transmission path between the transmitter and the receiver can vary from a simple direct path (Line Of Sight-LOS) to several indirect paths (Non Line Of Sight - NLOS) due to several obstacles (buildings, mountains, trees, *etc.*). The wave direction, the amplitude, phase and polarization are affected by these obstacles [25] that generate multipath between the transmitter and the receiver. The multipath phenomenon determines the main properties of the radio propagation channel [25]:

- time variability due to dynamic modifications of the radio propagation environment;
- spatial variability that describes a different behavior of the propagation channel when the transmitter and the receiver are moving. This provokes large and small scale variations of the signal called slow and fast fading (see Figure 2)
- frequency selectivity directly linked to multipath phenomenon impacts the transfer function in the frequency domain and by consequence, the impulse response in the time domain.

The multiple copies of a signal (rays) travel different paths with different propagation delays τ. These rays add constructively or destructively at the receiver, thereby giving rise to rapid fluctuations of the signal amplitude. This allows the reception of a signal even if there is no direct visibility between the transmitter and the receiver. Multipath provokes small scale variations that can reach several tens of dB. In addition, vehicle motion generates frequency shift called Doppler shifts, introduced on each path received. This creates a Doppler spectrum that affects the signal.

6.2.2 Longitudinal attenuation

The channel attenuates the power of the transmitted signal. One can consider the attenuation in line of sight accentuated by the masking effect linked to a curve or the presence of other vehicles and obstacles. Three types of attenuation exist:

- Large-scale attenuation, which corresponds to the average attenuation of the signal received over distances of a hundred wavelengths and appears classically in the link budget of a transmission [26]. The large scale variations expressed in dB follow a Gaussian law.
- The attenuation at medium scale, which corresponds to the variations of the received power over distances of the order of ten times the wavelength. It is caused mainly by the effects of masking the signal due to the various environmental obstacles present on the wave trajectory.

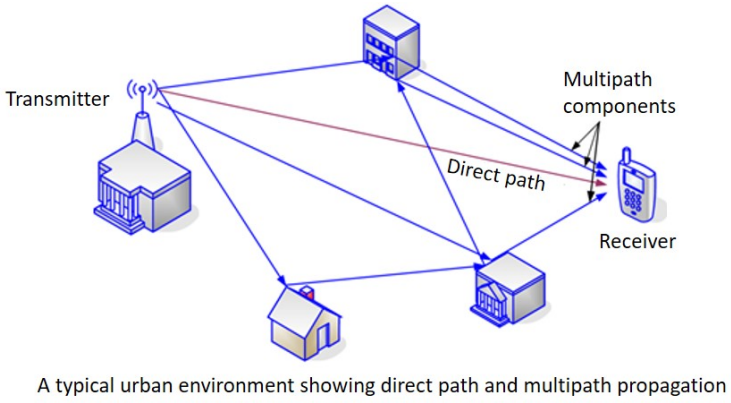

Figure 1: Illustration of multipath phenomenon

- The small-scale attenuation that corresponds to the fluctuations of the signal received over distances of the order of the wavelength. These variations are due to the physical phenomenon of multiple paths [27]. The well known small-scale variation laws are: Rayleigh for non line of sight reception, Rice for line of sight reception [24].

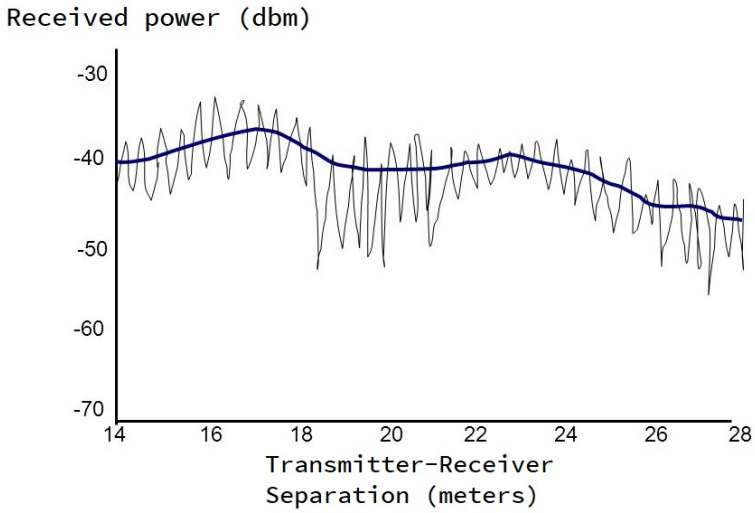

Figure 2: Illustration of slow and fast fading

6.2.3 Delay spread

The variation of the delay due to multipath can be statistically characterized. The delay spread corresponds to the variations of the delay around the mean value. The parameters that can be used to characterize the path delays in the channel are [28]:

- First-Arrival delay,
- RMS delay or deay spread,
- Mean excess delay,
- Maximal excess delay.

.

These parameters are illustrated in Figure 3 that represents the so called Power Delay Profile $P_h(\tau)$ at a given position, which represents the average power associated with a given multipath delay when a pulse is sent into the channel.

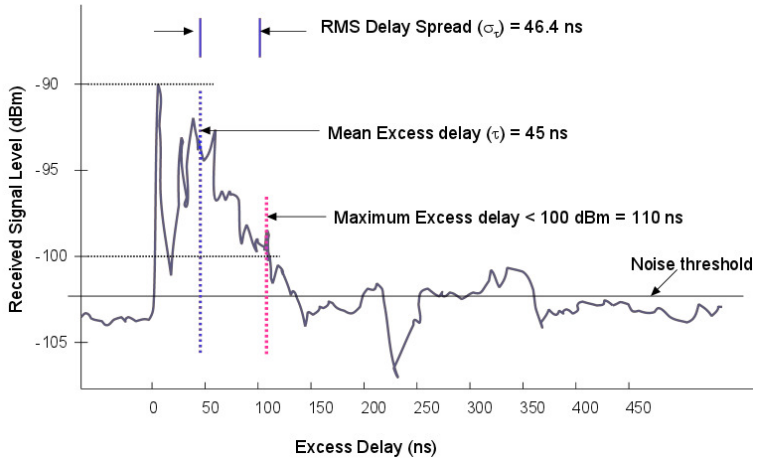

Figure 3: Illustration of Power delay profile measured

- **The First-Arrival Delay (τ_A)** is a time delay corresponding to the arrival of the first transmitted signal at the receiver. It is usually measured at the receiver. This delay is set by the minimum possible propagation path delay from the transmitter to the receiver. It serves as a reference, and all delay measurements are made relative to it. Any measured delay longer than this reference delay is called an excess delay.
- **The RMS Delay** (τ_{rms}) is referred to the second order moment (variance) of the mean excess delay.
- **The Maximum Excess Delay (τ_m)**, also called Maximum Delay Spread, denoted as τ_m, is the relative time difference between the first signal component arriving at the receiver to the last component whose power level is above some threshold. The RMS Delay spread is typically defined as (1):

$$\tau_{rms} = \sqrt{\frac{\sum_k P(\tau_k)(\tau_k - \overline{\tau})^2}{\sum_k P(\tau_k)}} \tag{1}$$

where

$$\overline{\tau} = \sqrt{\frac{\sum_k P(\tau_k)\tau_k}{\sum_k P(\tau_k)}} \tag{2}$$

where $P(\tau_k)$ represents the power associated to the k^{th} path. If the given Power Delay Profile values are continuous in terms of time delays, we replace the summation with integral and integrate it with respect to $d\tau$.

In the frequency domain, the channel coherence bandwidth is defined as Bc is proportional to $1/\tau_{rms}$ as a dual variable of τ_{rms}. B_c corresponds to the frequency band on which the transfer function of the channel can be considered as constant. On this frequency band, the spectral components of the signal are affected similarly. Both parameters are used to characterize frequency selectivity of a channel. When the signal bandwidth B_s is much lower than the coherence bandwidth $B_s \ll B_c$, the channel is considered as non selective in frequency. On the contrary, the channel is frequency selective. This resul inter symbol interferences (ISI). Channel selectivity impacts the system performance.

6.2.4 Doppler effect

Doppler effect refers to the shift of frequency of any radio signal due to the mobility. The Doppler shift f_d for the i^{th} path is proportional to the mobile speed v and the carrier frequency f_c. The Doppler equation for one ray is given by equation (3) [29]:

$$f_{d_i} = f_c \frac{v}{C} . \cos(\beta_i) \tag{3}$$

where f_c is the carrier frequency, C is the speed of light, v is the speed of the mobile, β_i is the arrival angle of the i^{th} path with the speed vector of the mobile.

Each path experiences a Doppler shift, then depending of the angle of arrival distribution, a Doppler spectrum is observed. If the angle of arrival are distributed between $[-\pi, +\pi]$ the Doppler spectrum can be expressed by equation (4) [30] and represented by Figure 4.

$$S(f) = \begin{cases} \frac{\sigma^2}{\pi f_d} . \frac{1}{\sqrt{1-\frac{f}{f_d}^2}}, & where - f_d \leq f \leq +f_d \\ 0, & otherwise \end{cases} \tag{4}$$

where σ^2 is the variance of the signal and f_d the maximal Doppler spread.

This Doppler spectrum is also known as *Classical* Doppler spectrum or *Jakes* Doppler spectrum illustrated in Figure 4. Depending on the distribution of the angles of arrival due to the environment but also due to the characteristics of receiving antenna, various Doppler spectrum shapes exist. The most well known are the *Flat* Doppler spectrum, the *Gaussian* and the *Rice* Doppler spectrum.

The time varying nature of the frequency dispersiveness of the channel in the time domain is characterized by the coherence time T_c which is inversely proportional to the Doppler spread.

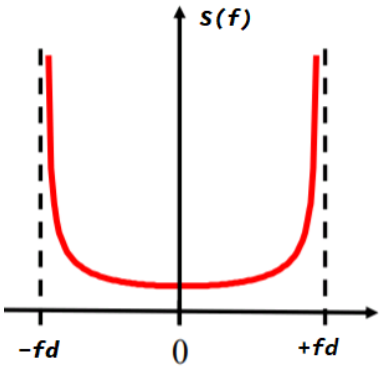

Figure 4: Representation of the Classic Doppler spectrum [2]

The Flat Doppler spectrum can be expressed by equation (5) [30] and represented by figure 5.

$$S(f) = \frac{1}{2f_d}, f_d \neq 0 \tag{5}$$

The Gaussian Doppler spectrum can be expressed by equation (6) [30] and represented by figure 6.

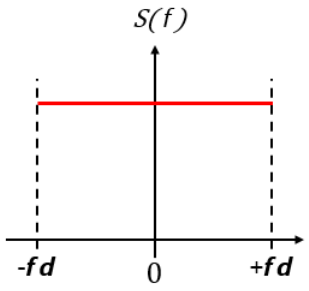

Figure 5: Representation of the Flat Doppler spectrum

$$S(f) = \begin{cases} \frac{1}{\sqrt{2\pi\sigma^2}} exp(\frac{f^2}{2\sigma^2}), & |f| \leq f_d \\ 0, & |f| > f_d \end{cases} \tag{6}$$

where $\sigma = \sigma_g.f_d$ with σ_g the standard deviation of the Gaussian classical function.

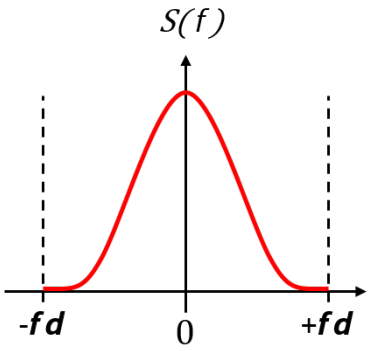

Figure 6: Representation of the Gaussian Doppler spectrum

The 3GPP-Rice Doppler spectrum can be expressed by equation (7) [30] and represented by figure 7.

$$S(f) = \begin{cases} \frac{0.41}{2\pi f_d} \cdot \frac{1}{\sqrt{1+10^9-(\frac{f}{f_d})^2}} + 0.91\delta(f - 0.7f_d), & |f| \leq f_d \\ 0, & |f| > f_d \end{cases} \tag{7}$$

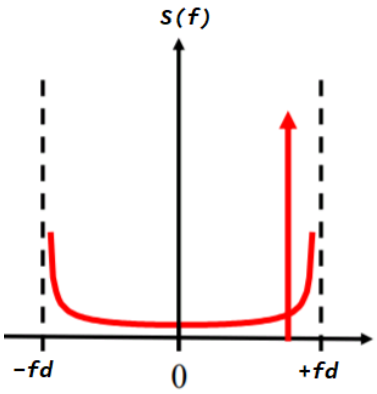

Figure 7: Representation of the Rice Doppler spectrum

7 Mathematical representation of wireless channels

The impulse response of the wireless channel is a broadband characterization of the channel that contains all the necessary information to analyze any type of radio transmission across the channel. This results from the fact that the mobile radio channel can be modeled as a linear filter. The filtering of the channel consists of the sum of the amplitudes and delays of several waves arriving at different moments of time. The baseband impulse response of the multipath channel can be expressed as (8):

$$h(t,\tau) = \sum_{n=0}^{N-1} c_n(t) \cdot e^{j2\pi \cdot f_{dn} \cdot t} \cdot \delta(\tau - \tau_n) \tag{8}$$

where c_n is the amplitude of the tap and f_{dn} is the Doppler shift of the n-th path.

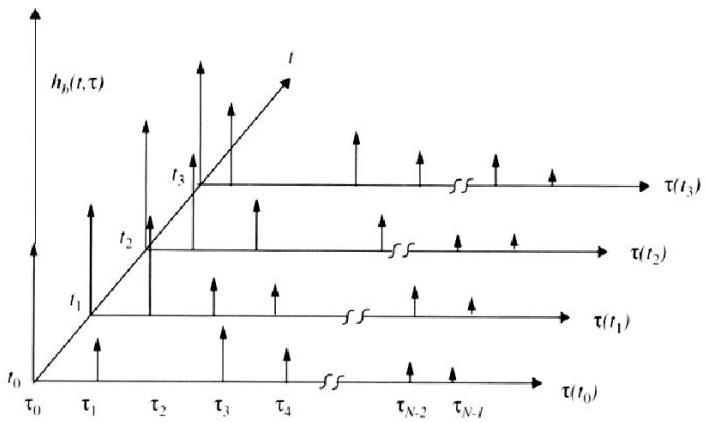

Figure 8: Time-varying impulse response representation

The time varying impulse response of the channel $h(t,\tau)$ is a two-variable function of t and τ. By taking the Fourier Transform (FT) of the impulse response with respect to the time delay variable τ and the time variable t, it is possible to build a set of four two-dimensional functions describing the channel in various forms. By applying to the impulse response a FT with respect to t, we obtain the Delay Doppler spread function. If a FT is applied to the impulse response but with respect to τ instead of t, we obtain the time-varying frequency response of the channel. A third system function called Doppler spread function is obtained by taking the FT of the frequency response with respect

to the time variable t.

The four system functions are known as $Bellofuntions$ [31]. $h(t,\tau)$ is the Impulse response, $H(t,f)$ is the transfer function or frequency response, $S(\tau,f_d)$ the Delay-Doppler spread function and $D(f,f_d)$ the Doppler spread function illustrated in Figure 9.

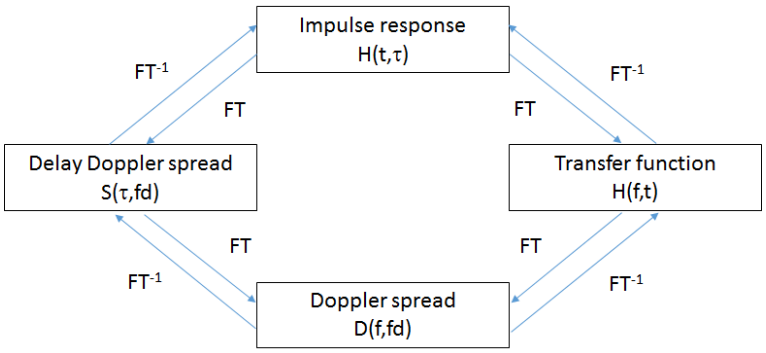

Figure 9: Bello functions

In order to characterize the stochastic process, the autocorrelation function (ACF) can be used. An autocorrelation function describes the similarity between a system function with delayed copy of itself over successive time intervals. The autocorrelation function of the channel impulse response is obtained by (9):

$$R_h(t,t';\tau,\tau') = E\{h(t,\tau)h^*(t',\tau')\} \tag{9}$$

where t and t' are time variables, τ and τ' are time delay variables, $*$ indicates the complex conjugate and E is the expectation value of the ensemble process.

From a general point of view, the output of the channel $y(t)$ can be expressed as the convolution of the complex channel impulse response and the input $x(t)$ [32] as (10):

$$r(t) = h(t,\tau) * s(t) + N(t) \tag{10}$$

where $r(t)$ and $s(t)$ denote the output signal and the input signal respectively. $N(t)$ is a white Gaussian noise.

7.1 Representation of the MIMO channel

A MIMO system is defined by the number of antennas at transmitter N_t side and the number of antennas at receiver side N_r. The classical representation of a MIMO channel relies on a channel description based on N_r x N_t independent SISO channels modeled with the **H** matrix. The equivalent diagonal matrix system allows expressing the channel as the superposition of several eigen-decorrelation channels. As recall in [33], it was demonstrated that the MIMO radio propagation channel is constituted of the superposition of several independent sub channels each carrying a fraction of the transmitted signal [9], [34]. The MIMO channel appears as a linear application of the emitted signal **X** towards the received signal **Y**. The singular value decomposition [35] of the **H** matrix allows the diagonalization of the linear system of equations. This singular value decomposition allows the diagonalization of the MIMO matrix system. The MIMO propagation channel can be modeled in two different ways. The first approach is to represent the MIMO propagation channel by a matrix of impulse responses containing all the impulse responses between each SISO link in the system.

When delays dispersion is greater than the symbol duration of the MIMO system, the impulse response of the channel are represented by several samples of K main propagation paths. The channel is large bandwidth. The impulse response matrix $\mathbf{H}(t)$ is expressed as the sum K channel matrices $\mathbf{H}_k$ each shifted of a delay τ_k as indicated in the following equation.

$$\mathbf{H}(t) = \sum_{k=1}^{K} \mathbf{H}_k \cdot \delta(t - \tau_k) \tag{11}$$

where $\mathbf{H}(t)$ is the channel matrix $(N_r \times N_t)$ modelling the channel characterised by K main paths and $\mathbf{H}_k$ is the matrix of $(n_r \times n_t)$ complex coefficients at instant τ_k such as (12) :

$$\mathbf{H}_k = \begin{bmatrix} h_{11}^k & h_{12}^k & \cdots & h_{1n_t}^k \\ h_{21}^k & h_{22}^k & \cdots & h_{2n_t}^k \\ \cdots & \cdots & \cdots & \cdots \\ h_{n_r1}^k & h_{n_r2}^k & \cdots & h_{n_rn_t}^k \end{bmatrix} \tag{12}$$

When the delays dispersion is very low compared to the symbol duration, the channel is considered as narrow band or non selective in frequency. The MIMO channel is perfectly described by the $(N_r \times N_t)$ channel matrix $\mathbf{H} = \mathbf{H}_1$ with complex coefficients in narrow band. Each complex coefficient represents the sum of all the received paths for a given position of both transmitter and receiver.

For a $N_r \times N_t$ MIMO system, where N_r and N_t are respectively the number of antennas at the transmitter and the receiver. The time variant MIMO matrix is defined by the equation (13):

$$H(t,\tau) = \begin{bmatrix} h_{11}(t,\tau) & h_{12}(t,\tau) & \dots & h_{1n}(t,\tau) \\ h_{21}(t,\tau) & h_{22}(t,\tau) & \dots & h_{2n}(t,\tau) \\ \vdots & \vdots & \ddots & \vdots \\ h_{m1}(t,\tau) & h_{m2}(t,\tau) & \dots & h_{mn}(t,\tau) \end{bmatrix} \tag{13}$$

Where $h_{mn}(t,\tau)$ is the SISO impulse response between the m^{th} transmitter antenna and the n^{th} receiver antenna.

The MIMO impulse response matrix, equation (13) can be used as a formalism of a MIMO input-output system between the transmitted signal vector $x(t)$ of size N_t and the vector of output signals $y(t)$ of size N_r as follows:

$$y(t) = \int_T H(t,\tau)x(t-\tau)d\tau + b(t) \tag{14}$$

Where $b(t)$ is the noise and interferences.

The second way to model the MIMO propagation channel is to represent the propagation channel by its doubly directional impulse response [36], [24] between the transmitter and the receiver. The doubly directional impulse response defined by Steinbauer and Molisch corresponds to the impulse response defined as follows.

In the case of MIMO, several antennas are used at the transmitter and the receiver to exploit the spatial diversity of the propagation channel. [37] shows that the Fourier analysis makes it possible to demonstrate the duality between space and wave in the same way as it exists between the time and frequency spaces [38]. The wave vector corresponds to the direction of propagation of a path. As a result, the impulse response of a MIMO channel between a pair of transceiver-receiver antennas can be written as:

$$h(t,\tau,\Omega_{BS},\Omega_{MS}) = \sum_{k=0}^{K-1} \alpha_k(t) exp(-j\Phi_k(t))\delta(\tau-\tau_k(t))\delta(\Omega_{BS}-\Omega_{BS,k}(t))\delta(\Omega_{MS}-\Omega_{MS,k}(t)) \quad (15)$$

Where $\Omega_{BS,k}$ and $\Omega_{MS,k}$ are the propagation directions of the kth path at the BS and MS respectively. Ω is a direction characterized by an azimuth angle φ and elevation angle θ as presented figure 10.

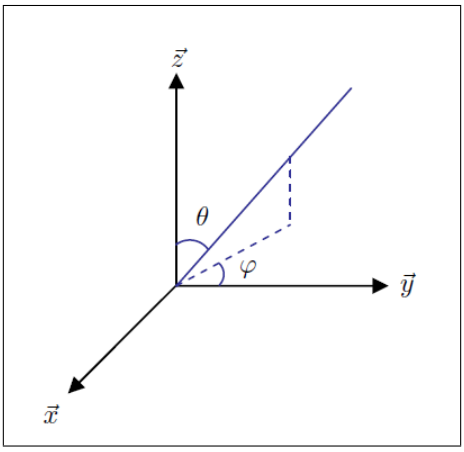

Figure 10: Representation of azimuth and elevation angles

The polarization diversity is taken into account by decomposing the impulse response according to the vertical and horizontal components. The impulse response of the radio propagation channel is then a matrix containing the different states of polarization (VV, VH, HH and HV) illustrated by equation (16):

$$h(t,\tau,\Omega_{BS},\Omega_{MS}) = \begin{bmatrix} h_{VV}(t,\tau,\Omega_{BS},\Omega_{MS}) & h_{VH}(t,\tau,\Omega_{BS},\Omega_{MS}) \\ h_{HV}(t,\tau,\Omega_{BS},\Omega_{MS}) & h_{HH}(t,\tau,\Omega_{BS},\Omega_{MS}) \end{bmatrix} \quad (16)$$

The propagation channel is completely described if there are the knowledge of the complex amplitude of each polarization states, propagation delay, direction of arrival at the BS and direction of arrival at the MS.

7.2 Wide Sense Stationary Channel (WSSUS) [[1]

The autocorrelation function depends on four variables, and is thus a rather complicated form for the characterization of the channel. Further assumptions about the physics of the channel can lead to a simplification of the correlation function. The most frequently used assumptions are the so-called Wide-Sense Stationary (WSS) assumption and the Uncorrelated Scatterers (US) assumption. A model using both assumptions simultaneously is called a WSSUS model. This assumption is very frequent even though it is far from reality. This assumption considers that over short periods of time or over small spatial distances, mobile radio channels are assumed to be stationary. Physically speaking, WSS means that the statistical properties of the channel do not change with time. Moreover, the channel response associated with a given multipath component of delay τ is uncorrelated with the response associated with a multipath component at a different delay $\tau' \neq \tau$, since the two components are caused by different scatterers.

7.3 Conclusion

In this section we have described the main features of the mobile wireless radio channel. We have introduced the channel impulse response that is used to model the wireless channel. In the following section we will present some well known mobile radio channel models.

8 Mobile Radio channel models

8.1 Introduction

The evaluation of wireless system performances requires to model the wireless channel. The models are generally based on mathematical representation of the impulse response of the channel. This topic is widely treated in the literature and the channel models are changing in relation with the increasing complexity of the communication systems. More and more parameters are taken into account in order to model radio channels as closed as possible to real channels. From a very general point of view, we can distinguish analytical, geometric and non geometric channel models.

Geometry based stochastic channel model (GBSCM) is a model that describes the statistics of the channel using a geometry representation of the physical environment and more particularly, a geometrical statistical description of the scatters. The GBSCM chooses scholastically the localization of scatterers following a certain distribution probability [39]. It exists three common techniques named: One Ring, Two Rings and Distributed scattering. The GBSCM is used by different organizations (3GPP, ITU, European projects) to model the channel in different scenarios. We can mention the spatial channel model (SCM) [40], [41], its extension (SCME) [42], WINNER [43], [7], [44], ITU-Advanced [10] and METIS [45].

The use of these types of radio channel models in the Emulradio4Rail platform required that all the geometric parameters can be implemented in the channel emulators. As we already explained in D2.1 [18] and D3.1 [21], the channel emulators used in the project can only implement the so called "Tapped Delay Line models". Consequently, in this deliverable, we will focus on the most simple ones, the non geometric stochastic channel model with the description of the Tapped Delay Line (TDL) channel model.

8.2 Non-Geometric Stochastic Channel Model

8.2.1 Introduction

A nongeometric stochastic channel model (NGSCM) is a model, which describes the paths between the transmitter and the receiver by statistical parameters. The geometry of the physical scenario is not taken in account. Two kinds of NGSCM can be found in the literature, the Tapped-Delay-Line (TDL) model that represents the channel by the definition of different paths in time/delay domain, and the Saleh-Valenzuela model, which represents the channel by a definition of clusters of paths in time/delay and angular domain, which is an extension of the TDL model. We will present the TDL model.

8.2.2 Tapped-Delay-Line channel model

The TDL channel model is a non geometric channel model that is a simple way to represent the channel impulse response in time domain. Indeed, the impulse response will be represented only by a discrete number of taps with their own time varying coefficients, amplitude and delay, as represented by the equation (17). The tap is represented by a Dirac delta function.

$$h(t,\tau) = \sum_{k=1}^{K} \alpha_k(t)\delta(\tau - \tau_k) \tag{17}$$

The impulse response $h(t,\tau)$ varies in time and is represented by the sum of all delayed taps. K represents the number of path, $\alpha_k(t)$ is an amplitude coefficient, δ is a Dirac delta function and τ_k is the arrival time of the path. This type of model assumes that the channel impulse response is a finite representation of the channel by the maximal number of paths K. Figure 11 gives a schematic view

of a four taps channel model.

An important remark is that α_k coefficients in (17) are related to each one of the taps and are not equivalent to c_n coefficients of the mobile channel model depicted in (8). The latter are associated to each multipath component in the receiver whereas the former are the amplitude of each one of the taps that form the model (and which may contain many multipath components). Therefore, the Doppler shift, which is addressed in (8) here it is not depicted in (17) because each one of the taps (which may have several MPCs) has its own independent Doppler Spectrum (and not only one shift).

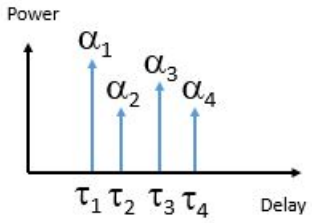

Figure 11: TDL representation of four taps

The resolution between two paths is limited by the bandwidth of the system as follows: $\delta t = \frac{1}{W}$ where δt is the maximal time resolution and W the bandwidth. For example, with a bandwidth equal to 20 MHz, the maximal time resolution is 50 ns. It is then possible to define a TDL with tap delays corresponding to the sampling times. The associated weight is then a sum of the complex path amplitudes contributing to the considered delay.

8.2.3 ITU models

The ITU models were developed by the IMT-2000 group to evaluate the IMT technologies like UMTS, LTE (3G) [46]. The purpose of these channels is to help system designers and network planners with a standard channel model to facilitate the system design and performance evaluation. The ITU model is used to model the time dispersion of the time variant wireless propagation channel as a Tapped Delay Line model. A set of four channel models is defined: Indoor office, Outdoor to indoor pedestrian, vehicular, Mixed-cell pedestrian/vehicular. The models are constructed to simulate the multi-path fading of a SISO channel with a 5 MHz of bandwidth at 2 GHz.

The multipath fading is modeled as a TDL with six taps with non uniform delay distribution. Each tap associates an amplitude characterized by a distribution (Rician with a K-factor $>$ 0, or Rayleigh with K-factor$=$ 0) and the maximal Doppler frequency. The recommendation specifies two different delay spreads for each test environment: low delay spread represented by 'A', and medium delay spread represented by 'B'. Each profile has a probability to emerge along time following the description in table 1. A more complex MIMO channel model based on Cluster Delay Line is given in [10].

Test environment	Channel A		Channel B	
	rms (ms)	P $(\%)$	rms (ms)	P $(\%)$
Indoor Office	35	50	100	45
Outdoor to indoor and pedestrian	45	40	750	55
Vehicular - High antenna	370	40	4000	5

Table 1: Probability of occurrence P in % for low delay spread and medium delay spread for each ITU scenarios [10]

The key parameters to describe each propagation scenario have to include: time delay spread, path loos and exceed path loss, shadow fading, multipath fading characteristics (Doppler spectrum), operating radio frequency.

The path loss model for vehicular environment is given by equation (18). The slow variation is considered as a log-normal distribution. This equation is given for urban and suburban area with a nearly uniform height for buildings.

$$L = 40.(1 - 4 \times 10^{-3}\Delta h_b).log_{10}R - 18log_{10}\Delta h_b + 21log_{10}f + 80 \quad (18)$$

where R is the distance between base station and mobile station in kilometer, f is the carrier frequency equal to 2 GHz and Δh_b is the base station antenna height in meters. The model is valid for Δh_b ranging from 0 to 50 m.

The slow fading over the distance implies that the adjacent fading values are correlated. The normalized autocorrelation function is approximated by an exponential function [47] as indicated by equation (19).

$$R(\Delta x) = exp(-\frac{|\Delta x|}{d_{corr}}ln2) \quad (19)$$

where Δx is the distance between fading and d_{corr} is the decorrelation length.

The scenario called *Vehicular B* is defined for a speed up to 120 km/h with a six taps TDL channel model. It is characterized by the number of taps, time delay relative to the first tap, average power relative to the strongest tap and Doppler spectrum as presented in the table 2.

Tap	Channel A		Channel B		Doppler spectrum
	Relative delay (ns)	Average power (dB)	Relative delay (ns)	Average power (dB)	
1	0	0.0	0	-2.5	Clasic
2	310	-1.0	300	0	Classic
3	710	-9.0	8 900	-12.8	Classic
4	1090	-10.0	12 900	-10.0	Classic
5	1730	-15.0	17 100	-25.2	Classic
6	2510	-20.0	20 000	-16.0	Classic

Table 2: ITU channel model for vehicular-A (30 km/h) and vehicular-B (120 km/h) scenarios [10]

8.2.4 Saleh-Valenzuela channel model

The Saleh-Valenzuela (SV) is originally developed for SISO wideband channel [48] and was further extended to MIMO system by including angle of arrival (AoA) [49]. The SV channel model is similar to the TDL model in term of using path representation with delay and magnitude identification. The SV channel model uses a definition of the so-called *cluster* representation. A cluster is a group of paths that comes from the same scatterer. This model defines the CIR of the channel with the following equation (20):

$$h(t,\tau) = \sum_{c=1}^{C-1}\sum_{k=1}^{K-1} \beta_{kc}exp(j\phi_{kc})\delta(t - T_c - \tau_{kc}) \quad (20)$$

where C is the cluster number, K the path number, β_{kc} is the real positive gain, ϕ_{kc} is the phase, T_c is the arrival time of the c^{th} cluster. The magnitude of path into a cluster is assumed to decrease following an exponential function. The same principle is assumed between cluster as shown in figure

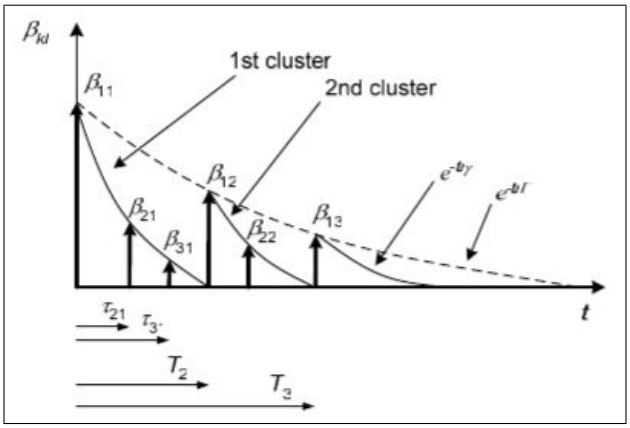

Figure 12: Saleh-Valenzuela representation following exponential decrease [3]

12.

With measurement campaigns presented in [50], it was found that the clusters are spread in time and also spread in angle of arrival. The SV channel model was extended to MIMO by adding angle of arrival statistics in equation (20). The corresponding equation is then given by (21):

$$h(t,\theta) = \sum_{c}\sum_{k} \beta_{kc} exp(j\phi_{kc})\delta(t - T_c - \tau_{kc})\delta(\theta - \Theta_c - \theta_{kc}) \tag{21}$$

where c is the c^{th} cluster, k is the k^{th} path in the cluster c and θ follows zero mean Laplacian distribution and Θ_c is uniformly distributed between 0 and 2π.

9 Radio channel models based on measurements and simulations in typical railway environments

9.1 Introduction

With the development of wireless communications in the railway domain, the development of channel models for railways is a very active field in a small community of researchers in the world. The authors generally considered Train to Ground (T2G), Train to Train (T2T) and intra-train communications for high speed train environments and also tunnels in the case of metro. The literature analysis shows that the majority of the papers are dealing with radio propagation models and they mainly present narrow band parameters such as path loss, fading statistics, angle distribution statistics and sometimes the delays and RMS delays distribution. We have also identified papers that present Tap delay Line and Cluster Delay lines models in different railway environments.

The main different railway environments are open environment or rural, viaduct, cutting, hilly terrain and tunnels. The main characteristics are given in D1.1 [19] of the Emulradio4Rail project. We will detail in this section the different TDL and CDL models identified in each type of environments in the case of T2G link. A specific section is devoted to high speed lines (HSL). In a different section, we will focus on the tunnel case. Table 3 presents a classification of the different papers found related to high speed lines and table 4 presents an equivalent classification for the tunnel scenarios. We will detail in the following subsections the main results extracted from the papers.

Scenario	Description of statistical propagation parameters (PL, K-factor, ...)	TDL models	CDL models	Incomplete models
Rural	[51], [52], [53],[54], [55] [56]	[12], [9]	[7], [10]	[52] [57] [58]
Viaduct	[59], [60], [61], [62]	[5], [11], [6]		[63]
Cutting	[64], [65], [60], [62]	[12], [66], [6]		[63]
Hilly terrain		[12], [14], [13]		
Station	[67]	[12]		[63]

Table 3: Classification of channel model for HSL from literature

Scenario	Description of statistical propagation parameters (PL, K-factor, AoA, AoD, ...)	Incomplete Saleh-Valenzuela model	Kronecker Weichselberger model	CDL model
Tunnel	[68], [69], [70], [71], [72], [73], [74], [75], [76], [77], [78], [79], [80], [81], [82], [83], [84], [85], [86], [86], [87]	[88]	[89]	[8]

Table 4: Classification of channel model for HSL from literature

9.2 Channel models obtained with measurements and simulations along high speed lines

9.2.1 Introduction

For some years now, journal papers presenting results of channel measurements along high-speed lines are quite numerous with the development of high speed train (HST) particularly in China. These environments are built to allow trains to run generally up to 350 km/h. Such a speed involves a lot of constraints for the measurements such as: large Doppler spread and fast variations of the channels parameters. A HST can, on a same line, pass over several scenarios. The high-speed environment can be classified into different scenarios: open space, viaduct, cutting, station and large tunnel [4]. The tunnel scenario will be considered in a following section. It is important to notice that there is not a lot of published papers referring to train-to-ground measurements along high speed line in Europe, the majority of the papers present results obtained along HSL in China.

As mentioned before, most of the results in the literature present the statistical properties of narrow band channel characteristics such as Path Loss and K-factor and distributions of angle of arrival or departure of the paths. In [51], [52], [12], [53], [54], [55] and [56], authors present results for various rural railway scenarios. A description of the radio propagation characteristics is given in [60], [59], [61] and [62] for viaduct scenario. The radio propagation characteristics in different cutting scenarios are described in [64], [65], [60] and [62]. An analysis of path loss and K-factor is performed in [67] for a station scenario.

In this report we decided to focus on wide band channel models that can be used for system evaluation, *ie* models that provide a description of the complex impulse response of the channel. Several TDL channel models are considered in [9] for rural scenario and also two CDL channel models in [7] and [10]. [5], [11] and [6] treated the case of viaduct scenario. [12], [66] and [6] deal with cutting scenario. [12], [14] and [13] present results for hilly terrain scenario and [12] for station scenario. We will present all these channel models starting with the TDL models then we will describe the CDL models.

9.2.2 Train to Ground Tapped Delay line channel model for high speed line scenarios

In [4], the high speed train geographical environment is divided in sub environments as illustrated in figure 13. We will follow this classification for the channel models.

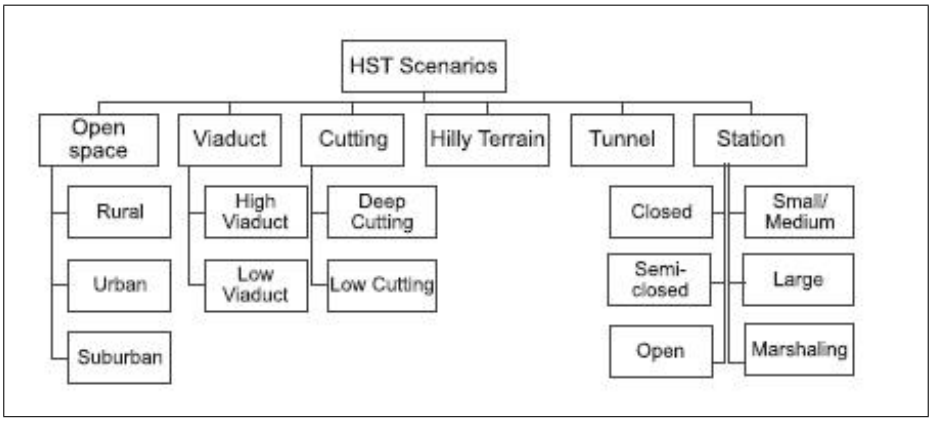

Figure 13: Classification of High Speed Train environments [4]

Open space scenario

This scenario is the most common HSL environment in China. If we consider T2G communications, the base stations are generally distributed along the tracks. Consequently, the LoS component is generally dominant between the transmitter and the receiver. As the distance between the transmitter and the receiver increases, the impact of the scatters becomes important and causes many multi-paths.

In [9], the authors present a measurement campaign in China between Beijing South Railway Station and Wuqing Station over 30 km. They considered public LTE FDD transmission. The speed of train is equal to 300 km/h. They use a NI-USRP 2952 (National Instrument-Universal Software Radio Peripheral) board as receiver to get channel information from LTE standard signal. The measurements are performed with SISO antenna configuration at 1.85 GHz with 20 MHz bandwidth and 30.72 MS/s sampling rate. Due to the bandwidth, the maximal delay resolution is equal to 0.06 µs. The maximal time delay which can be calculated is 11 µs because of the 90 kHz between two successive cell-specific reference signal (CRS). The receive antenna is located inside the train. The authors are able to define a two taps model for this open area scenario represented in the table 5. The characteristics of the antennas are not given.

Parameters	Value	
Center frequency	1.85 GHz	
Bandwidth	20 MHz	
Speed	300 km/h	
Antenna Configuration	SISO	
Path	Delay (µs)	Relative power (dB)
LOS path	0.2	-35.10
Second path	1.2	-49.60

Table 5: Two taps model for open area scenario at 300 km/h [9]

Viaduct scenarios

In viaduct scenarios the LoS component is dominant and the scatters have a minor impact on the receiver. In [5] a measurement campaign is performed in a viaduct scenario in China on Beijing-Tianjin HSL. The transmitter antenna is 3 m above the rail, on the top of the train and the receiver is located on the road at 83 m far from the viaduct as presented in figure 15. The antennas configuration is SISO with a wide band vertical-polarized Sencity Rail Antenna HUBER+SUHNER [90] transmit antenna and a dipole for the receiver antenna. The train speed is equal to 240 km/h and the receiver is an Elektrobit Propsound TM Channel Sounder working at 2.35 GHz with 10 MHz bandwidth. A direct sequence spread spectrum signal is used to extract the CIR with a length of 127 bits. Two Rubidium clocks are used to synchronize the transmitter and receiver. Authors divide the environment into five sub-regions related to the intersection point (IP) between the transmitting pylon and the track. The sub regions are defined depending on the average number of taps obtained in each sub region. They set up five corresponding TDL channel models for the viaduct scenario. The five areas are Remote Area (RA) with two paths, Toward Area (TA) with four paths, Close Area (CA) with eight paths, Closer Area (CEA) with three paths and Arrival Area (AA) into one tap. The number of path depends of resolvable multi-path components over the distance between the transmitter to the receiver. Each sub-region is defined by different number of path and relative time delay as illustrated table 6. The Doppler information is also presented. Variation in Doppler frequency becomes more severe when the track is close to Base Station (BS), and the rate of change is inversely proportional to the minimum separation between the track and the BS.

In [6], a measurement campaign is performed for a special scenario. Composed of 4 parts: a viaduct scenario situated between two cutting scenarios followed by a tunnel, as shown in figure 16. Here we focus only on the viaduct results. The measurements are performed for a SISO antenna

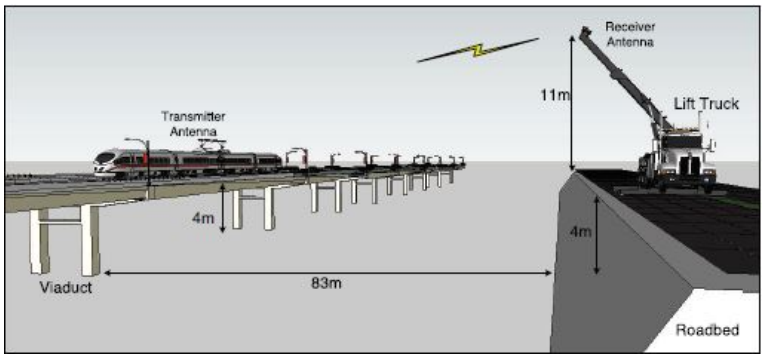

Figure 14: Description of viaduct scenario from [5]

Parameters	Value				
Center Frequency	2.35 GHz				
Bandwidth	10 MHz				
Speed	240 km/h				
Antenna configuration	SISO				
Scenario	Tap number	Relative time delay (μs)	Average path gain (dB)	K factor	Doppler shift
RA ($D_{CEA}+2300<D_s/2$)	1	0	0	K_{LOS_2}	f_{max}
	2	1.3	-13.7	K_{NLOS_1}	f_V
TA ($D_{CEA}+1300<D_s/2\leq D_{CEA}+2300$)	1	0	0	K_{LOS_2}	f_{max}
	2	0.6	-11.2	K_{NLOS_1}	f_V
	3	1.3	-14.9	K_{LOS_2}	f_V
	4	2.0	-15.9	K_{LOS_2}	f_V
CA ($D_{CEA}<D_s/2\leq D_{CEA}+1300$)	1	0	0	K_{LOS_2}	f_{max}
	2	0.5	-12.9	K_{NLOS_1}	f_V
	3	1.2	-15.7	K_{NLOS_2}	f_V
	4	1.6	-18.9	K_{NLOS_2}	f_V
	5	2.0	-20.8	K_{NLOS_2}	f_V
	6	3.1	-19.8	K_{NLOS_2}	f_V
	7	3.5	-21.3	K_{NLOS_2}	f_V
	8	5.6	-21.0	K_{NLOS_2}	f_V
CEA ($D_{AA}<D_s/2\leq D_{CEA}$)	1	0	0	K_{LOS_1}	f_d
	2	0.4	-15.2	K_{NLOS_1}	f_V
	3	1.2	-19.7	K_{NLOS_1}	f_V
$AAD_s/2\leq D_{AA}$	1	0	0	K_{LOS_1}	f_d

Notes
(1) $D_s/2$ is the initial distance of the train from IP in meters, both 1300 m and 2300 m are empirical values based on experimental results;
(2) $K_{LOS_1}=-0.0337d+23.05$, $K_{LOS_2}\sim N(8.25,1.05^2)$, $K_{NLOS_1}\sim N(5.9,1.5^2)$, $K_{NLOS_2}\sim N(1.7,0.2^2)$;
(3) $f_V\in 0.5f_{max},0.7f_{max},0.9f_{max}$ with probabilities of 9%, 43% and 48%; $f_d(t)=f_{max}cos(\theta(t))$ with θ : arrival angle of receiver;
(4) In the Adjacent Area (AA), according to the arriving or departing process, two K_{LOS_1} piece-wise linear models with a positive or negative slope can be obtained;

Table 6: TDL channel model for viaduct scenario with f_{max} equal to 524 Hz [5]

configuration where the transmitter is 20 m away from the tunnel entrance at 35 m high. The transmitting antenna is a directional L-Com HG72714P-090 panel with vertical polarization with 17 °vertical and 90 °horizontal beam width. The receiving antenna is a L-Com HG72107U vertically polarized. The omnidirectional receiving antenna moves along the track. The channel sounder uses a narrow pulse technology with a pulse period of 1 µs. Pulse width is equal to 30 ns, 45 ns and 60 ns. Two frequencies are investigated: 950 MHz and 2150 MHz. The sampling interval is 50 ns. Authors are able to provide a TDL channel model for two regions, near cutting 1 and near cutting 2 as shown in table 7. This channel model is validated by a Ray-tracing method which considers the same geometrical parameters as the measurement campaign performed at 310 km/h. The authors investigate the correlation coefficients between delay and Doppler. For viaduct scenario the correlation coefficient equals 0.0308 and 0.0143 respectively for 950 MHz and 2150 MHz.

In [11], another measurement campaign is performed for viaduct scenario on Harbin-Dalian HSL. The measurements are performed for a 2x2 MIMO configuration where the transmitter is 15 m away from the viaduct at 40 m height. The transmit antenna is omnidirectional with 45 °of vertical polarization with 65 °and 7 °vertical beam width. The receiving antennas are positioned on the roof of the train with a distance of 0.5λ. The sounding signal is a M-sequence with a length of 1023 using Binary Phase Shift Keying (BPSK) modulation. The measurement campaign is performed at 2.6 GHz with

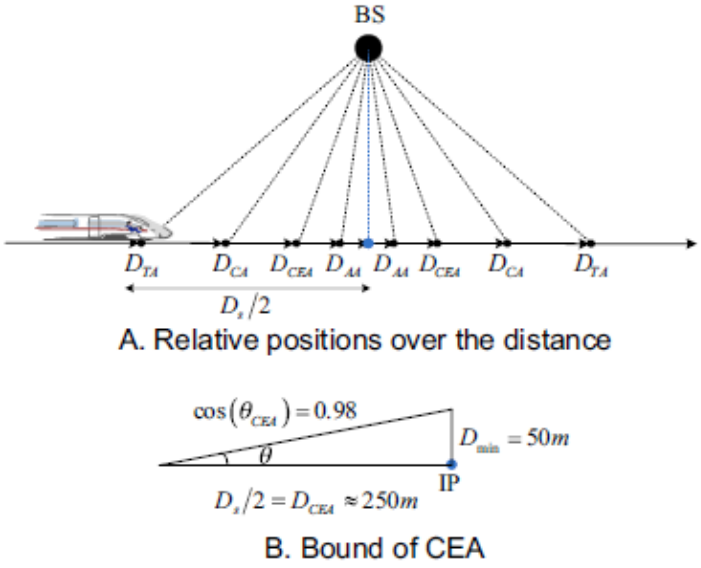

Figure 15: A - Relative positions over the distance. The blue dashed line denotes D_{min}, the blue point represents IP of D_{min} and the rail. D_{AA}, D_{CEA}, D_{CA} and D_{TA} are the distances from IP to the corresponding area bound, respectively. B - Schematic illustration of D_{CEA} . [5]

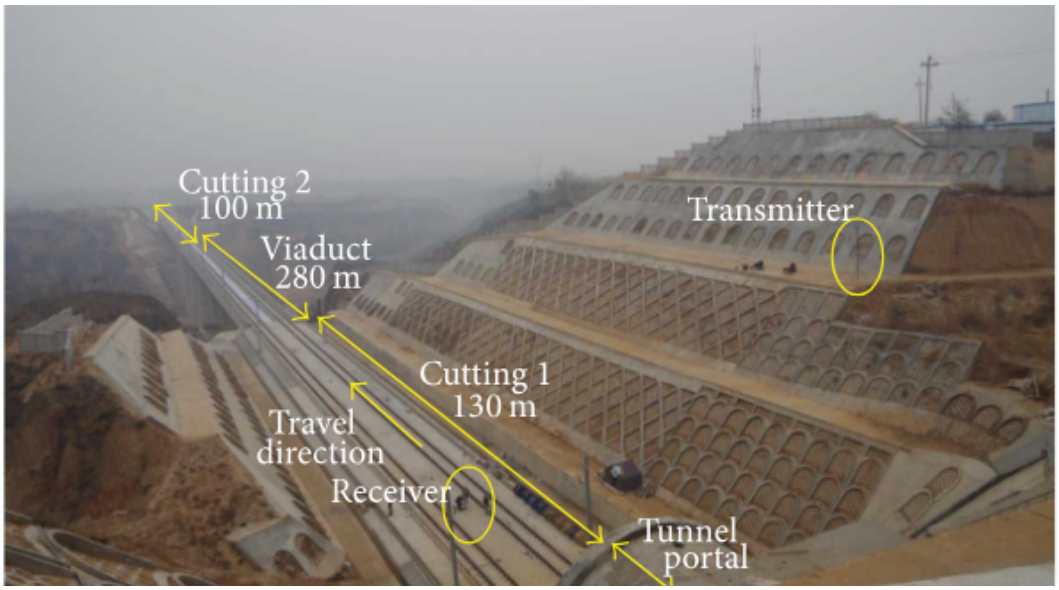

Figure 16: Description of viaduct scenario from [6]

a 20 MHz bandwidth. The train speed is equal to 370 km/h. Two Agilent N9020 spectrum analyzers are used with a sampling rate of 19.53 ns. Contrary to the viaduct TDL models presented before, this model does not define sub-regions and provide a four taps delay model as described in Table 8. The mean RMS delay equals 203 ns higher than the one obtained with WINNER II channel model for LOS rural environment.

Cutting scenarios

In cutting scenario, a measurement campaign was performed on Beijing-Tianjin HSL [12] as illustrated in figure 17. The authors use R&S TSMQ Radio Network Analyzer to extract the resolvable multipath component with a maximal resolvable time delay of 20 µs. A SISO antenna configuration is

Parameters	Value			
Center frequency	950 MHz		2.15 GHz	
Bandwidth	20 MHz		20 MHz	
Speed	310 km/h		310 km/h	
Antenna configuration	SISO		SISO	
Scenario	Delay (µs)	Relative power (dB)	Delay (μs)	Relative power (dB)
Near cutting 1	0	0	0	0
	108.3	-37.27	106.5	-22.95
			428.4	-39.6
Near cutting 2	0	0	0	0
	89.5	-9.5	107.3	-21.46

Table 7: TDL model for viaduct scenario [6]

Parameters	Value	
Center frequency	2.6 GHz	
Bandwidth	20 MHz	
Speed	370 km/h	
Antenna configuration	MIMO 2X2	
Taps	Delay (ns)	Relative power (dB)
1	0	0
2	78	-4.304
3	195	-6.523
4	332	-9.468

Table 8: 4 Taps channel model for viaduct scenario [11]

used to sound the channel signal using both WCDMA signal at 2.4 GHz with 5 MHz bandwidth at 240 km/h. The transmitter antenna is at 30 m away from the track on the top of the one slope wall. The receive antenna is on the roof of the train. The antenna characteristics are not given. The authors provide a four taps TDL channel model of this cutting scenario illustrated by the Table 9 with a Classical/Rice Doppler spectrum distribution for the first tap and a classical Doppler spectrum distribution for the others.

An other model for cutting is proposed in [6]. The measurements have been described previously. The environment refer to figure 16. The corresponding TDL model is given in table 10.

Figure 17: Illustration of U-shape cutting scenario corresponding to the TDL model given in table 9

Hilly terrain scenarios

Parameters	Value	
Center frequency	2.4 GHz	
Bandwidth	5 MHz	
Speed	240 km/h	
Antenna configuration	SISO	
Taps	Delay (ns)	Relative power (dB)
1	0	0
2	300	-7.3
3	900	-22.9
4	2100	-24

Table 9: TDL channel model for cutting railway scenario [12]

Parameters	Value			
Center frequency	950 MHz		2.15 GHz	
Bandwidth	20 MHz		20 MHz	
Speed	310 km/h		310 km/h	
Antenna configuration	SISO		SISO	
Scenario	Delay (µs)	Relative power (dB)	Delay (μs)	Relative power (dB)
Cutting 1	0	0	0	0
	82.9	-36.86	95.7	-32.16
	138.1	-51.26	180.4	-55.39
	192.6	-52.93	254.7	-57.35
	241.4	-55.66	305.1	-55.71

Table 10: TDL model for cutting scenario [6]

This environment is densely scattered with objects distributed irregularly and non uniformly. With high altitude transmit antennas and low-altitude obstacles, the LoS component is observable and it can be detected along the entire railway line. However, multi path components scattered/reflected from the surrounding obstacles will cause serious constructive or destructive effects on the received signal and therefore influence the channel's fading characteristics [91].

In [13], a TDL model is proposed for hilly scenario with a train speed equal to 295 km/h at 2.4 GHz with 40 MHz bandwidth on Guangzhou-Shenzhen HSL using Tsinghua University (THU) channel sounder [92]. The transmitted signal is a linear frequency modulated sequence (LFM) of length 12.8 µs. The transmitter antenna is a directional antenna and is located at 10 m far from the railway track and 30 m high. The receiver antenna is omnidirectional and is placed on the roof of the train. Subspace Alternating Generalized Expectation (SAGE) algorithm is used to extract the multi path component. Authors divide into four sub-regions, the hilly terrain scenario depending of the number of predominant paths in each area: Remote Area (RA) with three paths, Distant area (DA) with five paths, Close Area (CA) with thirteen and Adjacent Area (AA) with three paths. Four TDL channel models are set up as presented in table 11.

In [14], a measurement campaign, in hilly terrain at 2.6 GHz with 20 MHz of bandwidth along the Harbin-Dalian HSL at 370 km/h is studied. A 1023 bit length pseudo noise (PN) sequence modulated by a BPSK generated by Agilent E4438C VSG is used. The antenna configuration is SISO one where the transmitter antenna is fixed on the operator BS. This antenna is a cross-polarization directional antenna with 65°horizontal and 6.8°vertical beam width. The receiver antenna is omnidirectional placed on the roof of the train. The authors defined two sub-regions with different number of predominant paths: near region and far region and they defined for each a TDL model as illustrated on table 12.

In [12], a measurement campaign is performed in hilly terrain scenario on Beijing-Tianjin HSL. The scenario is composed by a plain environment on one side and a mountain at a distance of 800 m on the other side. The environments studied are plain, hilly terrain, U-shape cutting and station scenario.

Parameters	Value			
Center Frequency	2.4 GHz			
Bandwidth	40 MHz			
Speed	295 km/h			
Antenna configuration	SISO			
Scenario	Tap number	Relative time delay (ns)	Average path gain (dB)	Doppler shift
AA	1	0	0	- f_{max}
	2	280	-8.7	f_V
	3	640	-17.5	f_V
	4	1350	-27.2	f_V
CA	1	0	0	- f_{max}
	2	200	-11.4	f_V
	3	450	-27.6	f_V
	4	520	-12.7	f_V
	5	860	-29.0	f_V
	6	1160	-28.0	f_V
	7	1230	-27.6	f_V
	8	1330	-23.8	f_V
	9	1390	-23.1	f_V
	10	1480	-25.9	f_V
	11	1590	-18.7	f_V
	12	1770	-29.1	f_V
	13	2100	-29.7	f_V
DA	1	0	0	- f_{max}
	2	230	-9.2	f_{max}
	3	1.2	-15.7	f_{max}
	4	1.6	-18.9	f_{max}
	5	2.0	-20.8	f_{max}
RA	1	0	0	- f_{max}
	2	0.4	-15.2	f_{max}
	3	1.2	-19.7	f_{max}

Notes
(1) f_V is a random variable and $f_V \sim$ U [- f_{max},+ f_{max}].
(2) The Doppler shift values are corresponding to the case when the train departs from the intersection point.

Table 11: TDL channel models for hilly terrain sub-regions [13]

Parameters	Value		
Center frequency	2.6 GHz		
Bandwidth	20 MHz		
Speed	370 km/h		
Antenna configuration	SISO		
Scenario	Delay (ns)	Relative power (dB)	Doppler shift*
Near region	0	0	f_{max}
	97.65	-6.77	$0.5.f_{max}$
	216.79	X	$0.5.f_{max}$
Far region	0	0	f_{max}
	78.12	-3.23	$0.5.f_{max}$
	175.77	-7.79	$0.5.f_{max}$
	234.36	-11.60	$0.5.f_{max}$
	312.48	-16.55	$0.5.f_{max}$

Table 12: TDL channel model for near and far region of hilly terrain with f_{max} equal to 875 Hz [14]

Here we focus only on the hilly terrain scenario. The authors use R&S TSMQ Radio Network Analyzer to extract the resolvable multipath component with a maximum resolvable time delay of 20 µs. A SISO antenna configuration is used to sound the channel signal using both WCDMA signal at 2.4 GHz with 5 MHz bandwidth at 240 km/h. The transmitter antenna is at 30 m away from the track on the top of the one slope wall. The receive antenna is on the roof of the train. The authors provide a three taps TDL channel model of this hilly terrain scenario illustrated by the table 13 with a Classical/Rice Doppler spectrum distribution for the first tap and a classical Doppler spectrum distribution for the others.

Parameters	Value	
Center frequency	2.4 GHz	
Bandwidth	5 MHz	
Speed	240 km/h	
Antenna configuration	SISO	
Scenario	Delay (μs)	Relative power (dB)
	0	0
	0.3	-7.6
	0.6	-22

Table 13: TDL model for hilly terrain [12]

Station scenario

In the same paper as before [12], authors defined a three taps TDL channel model for the station scenario presented in table 14. The Doppler distribution is the same as before.

Parameters	Value	
Center frequency	2.4 GHz	
Bandwidth	5 MHz	
Speed	240 km/h	
Antenna configuration	SISO	
Taps	Delay (μs)	Relative power (dB)
1	0	0
2	0.3	-5.2
3	0.6	-8.2

Table 14: TDL model for station scenario [12]

9.3 Train to Ground Cluster Delay line channel model for high speed line scenario

The CDL channel model represents a channel formed by several clusters of taps, which represent paths with different delays and angle of arrival. Due to the complexity to defined a CDL channel model, the literature is poor in term of complete CDL channel model in the railway domain. At the moment of the writing of the report, only two CDL channel model have been found for rural scenario: the WINNER II channel model D2a [7] and the IMT-A MRa channel model [10].

The Deliverables D1.1.2 V1.0 [15] and V1.2 [16] of WINNER II project related to channel models present a typical open rural area scenario for high speed line. The frequency range is from 2 GHz to 6 GHz with a bandwidth up to 100 MHz. The antennas (Huber+Suhner rooftop antenna SWA 0859 – 360/4/0/DFRX30 - 5.25 GHz) are located on the roof of the train. The measurements were performed with Propsound multi dimensional radio channel sounder from Elektrobit. This scenario is available for a speed of 350 km/h using Moving Relay Stations (MRS) on the train at 2.5 m high and with the BS at 50 m away from the track at 30 m high every 1 000-2 000 m. This scenario is presented on the figure 18. For this WINNER II model, the total number of paths in a cluster is set at 20. While the total number of clusters is given by N = 8. Since the scenario is set in a rural area, the NLOS case is not considered.

The model is expressed as CDL channel model. The parameters of LOS condition are given in table 15. In the LOS model Ricean K-factor is 7 dB. The deliverables also give all the propagation parameters for the D2a scenario.

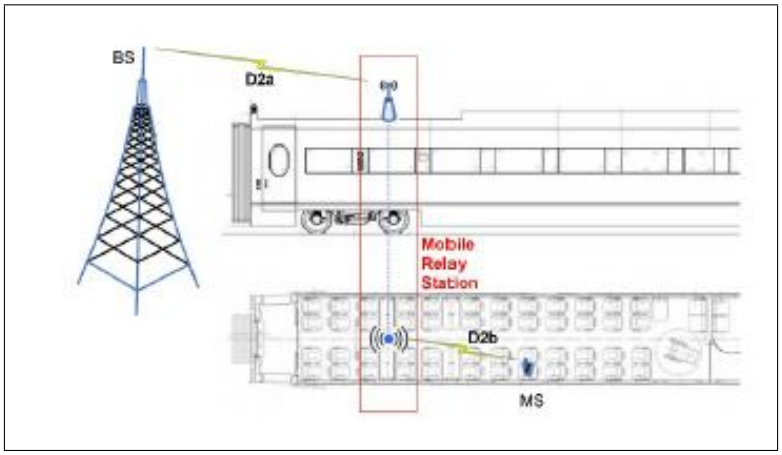

Figure 18: D2a scenario [7]

The guidelines for evaluation of radio interface technologies for IMT-Advanced is also presented in [10]. A model composed by a rural macro (RMa) cell scenario is referred as the typical open rural railway scenario. The frequency range, only for this RMa scenario, is from 450 MHz to 6 GHz with a bandwidth up to 100 MHz. A High Speed Line scenario is defined as B3 scenario for a train speed up to 350 km/h. This scenario covers a wide area, which can be up to 10 km. The BS antenna height is generally in the range from 20 to 70 m. Two CDL channel models are given for the RMa channel model, the LOS and NLOS ones. This paper also defines all the path loss parameters for the RMa scenario.

9.3.1 Conclusion

In this chapter we presented the main results found in the literature regarding radio channel models in HSL scenarios that can be considered to evaluate system performances (able to be implemented

Parameters	Value									
Center frequency	2-6 GHz									
Bandwidth	Up to 100 MHz									
Speed	350 km/h									
Antenna configuration	SISO-MIMO									
Cluster number	Delay (ns)			Relative Power (dB)			AoD (°)	AoA (°)	Ray power (dB)	
1	0			0.0			0.0	0.0	-0.12*	-28.8**
2	45	50	55	-17.8	-20.1	-21.8	12.7	-80		-27.8
3	60			-17.2			-13.6	86		-30.2
4	85			-16.15			13.4	84.4		-29.5
5	100	105	110	-18.1	-20.4	-22.1	-13.9	87.5		-28.1
6	115			-15.7			-13	-82.2		-28.7
7	130			-17.7			-13.9	87.5		-30.8
8	210			-17.3			13.7	86.2		-30.3
* power of dominant ray ** Power of each other ray Cluster ASD = 2° Cluster ASA = 3° Cross polarisation XPR = 12 dB										

Table 15: CDL parameters channel model for D2a scenario [15] et [16]

for example in a radio channel emulator). The analysis conducted shows that there are a lot of papers dealing with a representation of some statistical channel parameters as path loss, K-factor, angle of arrival, etc. but there are not a lot of complete channel models that give a representation of the complex impulse response of the channel. A quite general and straightforward methodology to implement channel model is the TDL model. We provide a review of some TDL channel model for rural, viaduct, cutting, hilly terrain and station scenarios. It is shown that, for a same scenario, different channel models can be defined depending of the number of representative paths for example. An other channel model that can be found in the literature is the CDL channel model which is more complex than TDL channel model. There are not a lot of CDL channel model in the literature due to the complexity of model. We are able, for now, to describe only two CDL channel model. The first one is presented in the WINNER II model created by the 3GPP. The second on is presented in the IMT-A model created by ITU. Both of them describe a CDL model for rural scenario. No more CDL channel model has been found for other HSL scenario in the literature.

9.4 Channel models obtained with measurements and simulations in tunnels

9.4.1 Introduction

As mentioned in the introduction of this part, most of the results in the literature present the statistical properties of narrow band channel characteristics such as Path Loss and K-factor and distributions of angle of arrival or departure of the paths [68]-[87].
As for the high speed line part, we decided to focus on channel models that can be used for system evaluation, *ie* models that provide a description of the compex impulse response of the channel. The literature in this part is not studied a lot. In [88], a Saleh-Valenzuela channel model is identified with two main clusters. However, these papers do not give enough information about them to use it as a reference channel model. In [89], the authors focused on the Kronecker and Weichselberger channel models. Finally, [8] provides a CDL channel model based on the WINNER procedure using a ray tracing method.

In this part, we will introduce firstly, the free propagation in tunnel environment. Then, we will give the channel models that we found in literature regarding the train to ground channel model for tunnel scenario. A CDL channel model will be also given following the WINNER approach. Finally, a TDL channel model will be defined for the train to train communications in case of inter-consist and intra-consist communications. Both of the inter-consist and intra-consist communications will be explain in the last section.

9.4.2 Free propagation in tunnel

Radio propagation inside the tunnel is affected by several phenomena that will affect the signal propagation:

- wave guide effect created by the tunnel walls that act as an oversize wave guide in certain conditions as mentioned before;
- multiple reflection on the tunnel walls and diffraction on the edge that create fast variations and fading of the electromagnetic field inside the tunnel;
- an attenuation and a coupling between the inside and the outside of the tunnel that depends on the position of the radio access point versus the tunnel axis;
- masking effects related to the presence of other trains inside the tunnel, the existence of curves or discontinuities (enlargement - narrowing) inside the tunnel.

From a general point of view, the traditional free space radio wave propagation laws are no more valid in tunnels. When the tunnel length can be considered as infinite without curve, if the tunnel is not metallic and if the dimensions of the transverse section of the tunnel are large compared to the wavelength of the operating signal, the tunnel can be considered as an oversize dielectric wave guide [93]. In this case, there are different approaches and methodologies to describe radio wave propagation in tunnels. The objective of the different existing methodologies is to express the complex electromagnetic field in the confined area thanks to the resolution of Maxwell equations with specific boundary conditions imposed by the characteristics of the tunnel walls.

The most used methods are: rigorous description by solving Maxwell equations [94] with mathematical methods (integral methods or parabolic vector equations [95], [96], [97]), asymptotic approach to solve the equations by using the optical approximation using ray tracing [98], [99], [100], [77] and

[87] or ray launching [101]. The modal theory is also often considered and permits physical interpretation of some phenomenon [94]. [102] and [93] have developed the electromagnetic field equations in the case of rectangular linear tunnel. The case of circular tunnel was treated in [103] and [104]. More details can be found in [101] and [105]. This theory allows to express the electromagnetic field for rectangular and circular infinite linear tunnels.

Between 1 to 10 GHz, the tunnel walls (in concrete for example) behave as low loss dielectric material with the dielectric constant ϵ varying between 5 and 10 and with dielectric conductivity. The permittivity σ varies between 0.01 and 0.06 S/m. In this case, the propagation of an electromagnetic wave inside an infinite of tunnel with a rectangular cross section and with dielectric walls is the consequence of the existence of an infinity propagation modes called hybrid modes EH_{mn}. All these modes are lossy modes because the reflections on the walls imply that a part of the signal is refracted inside the wall and an other part is reflected on the wall. The consequence is a power decrease with propagation inside tunnel.

Figure 19 illustrates the evolution of the electric field attenuation along the tunnel obtained with a ray tracing tool at 800 MHz, 900 MHz, 2.45 GHz, 4 GHz and 5.8 GHz. This figure shows the strong influence of frequency. Other parameters such as the tunnel section and the presence of an other train or not will influence the path loss inside the tunnels.

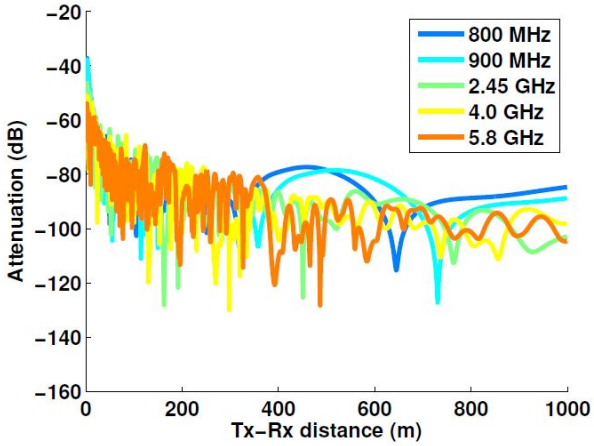

Figure 19: Evolution of the electric field along tunnel for different frequencies

Recent papers present results obtained thanks to narrow band measurements or ray tracing simulations. Table 4 given in section 9.1 presents a classification of the different papers that we will detail in the following paragraphs. We recall that in this study we focus on papers that present channel models that can be considered to evaluate performances (expression of the complex impulse response of the channel).

Most of the measurement campaigns in tunnel are performed at 900 MHz, 2.4 GHz and 5.8 GHz which correspond today to the frequency bands considered for railway communications systems [70], [84], [86],[88], [106], [107], [108], [82] and [78] highlight only on large scale fading parameters. In [82] a MIMO configuration is used to defined also the PL, PDP, K-factor and delay spread channel characteristics at 2.1376 GHz.

Some general remarks for MIMO case in tunnels

It is important to note the particularity of the case of MIMO (Multiple Input Multiple Output) systems in tunnels. [109] highlighted the decorrelation observed due to interference between the various hybrid modes. In [110], the hypothesis of the authors is that modal diversity can be compared to spatial diversity for MIMO techniques. Depending on the transverse or longitudinal receiver position in the tunnel, different modes EH_{mn} can be excited. This hypothesis was confirmed in [111]. In [89], the authors have illustrated very clearly the influence of the hybrid modes excitation on a MIMO system performance. Using ray tracing simulations in a straight tunnel with rectangular cross section, they highlighted that when the antennas are perpendicular to the tunnel longitudinal axis, the MIMO channel capacity is maximal. In contrary, when the antennas are parallel to the longitudinal axis, the MIMO channel capacity is minimal. These results have been also confirmed in underground mines by [112], [113], [114] and in railway tunnels by [108].

Keyholes phenomenon was highlighted by [115]. This phenomenon occurs when the distance between the transmitters and the receivers is large compared to the radius of the circle in which the scatters at transmission and receptions sides are situated [116]. This phenomenon exists when the signals propagate in a corridor or a tunnel or when the transmitter ans receiver are very far to each other in outdoor. These channels are degenerated and can be represented by a channel matrix of rank 1 despite a total decorrelation.

The existence of a keyhole highlight the fact that a certain position in the channel, all the paths are correlated. In this case, the channel matrix is degenerated with only one degree of freedom (only one non zero eigenvalue). This is very negative for MIMO performances. In [117], the authors analyze the probability of presence of keyholes [118], [119] in various tunnel types (old and new ones). They showed the big influence of tunnel dimensions and changes in the cross section dimension as well as the fact that the tunnel is new or not. Paradoxically, the presence of keyholes does not impact the capacity[117].

In [120] the authors analyze the influence of the variations of dimension of the tunnel transverse section on the probability of presence of keyhole. References to keyhole effects appear also in [121], [110], [122]. Generally, the higher is the correlation between the signals, the lower is the channel capacity. Nevertheless, when the correlation between antennas is low, the channel matrix $\mathbf{H}$ presents a low rank (equal to 1) and a keyhole phenomenon can occur. The example generally chose, is a scenario with a small hole in a wall that separates the environment between transmitter and receiver. The mathematical description of the phenomenon is given in [119].

9.4.3 Train to Ground channel model for tunnel scenario

As illustrated in table 4, only two papers give all the parameters of the models for T2G transmissions. At the moment of writing this report, we identified a Saleh-Valenzuela representation in [88] where authors defined two clusters but do not provide information on the various parameters to use it. Thus, we will not take it into account. The Kronecker and Weichselberger models based on correlation can also be considered for performance evaluations as presented in [89] but it is difficult to consider them for channel emulation. Finally, a WINNER CDL channel model is defined in [8].

WINNER CDL channel for tunnel environment

Only one channel model based on WINNER channel model has been set up in [8] at 5.8 GHz. The model was obtained using a Ray-Tracing tool to simulate free propagation in a given realistic dynamic scenario with two tracks and two trains. The four receiving antennas patch are fixed on the roof of the moving train. The scenario is represented figure 20. The simulated train was running at 50 km/h. The authors present a 4x4 MIMO model based on 5 clusters. Each path of each cluster is defined in terms of delay, power, AoA and AoD.

We consider that the transformation of a CDL model into a TDL one is not straightforward, so this reference [8] will not be considered for emulation. Therefore, the only remaining solution could be to generate a proper TDL model from scratch using ray-tracing simulations. This option is not considered for the moment.

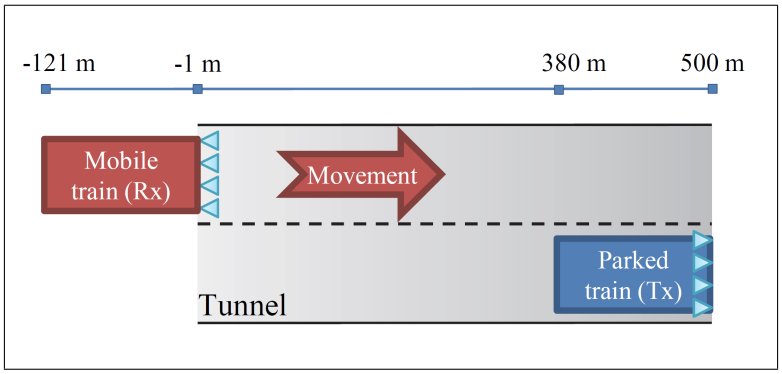

Figure 20: Representation of the scenario simulated [8]

9.4.4 Conclusion

Today, the literature analysis conducted shows that there is no available general MIMO channel model to describe the behavior of dynamic subway scenario in tunnel from a radio channel point of view in order to evaluate digital communication system performances. In this section we highlighted the main results found in the literature regarding channel models in tunnels that can be considered to evaluate system performance. This topic is not yet intensively treated in the literature. A lot of papers dealing with statistical analysis of measurements in the 2-5 GHz band can provide some results on fadings and delay spread statistics. Several papers also analyze the variation of the spatial correlation degree in the tunnel as a function of antenna polarization or antenna positions. Based on this figures, it is possible also to build simple statistical models such as Kronecker and Weichselberger models. Another channel model is a WINNER CDL channel model obtained with dynamic simulations based on an optimized ray-tracing simulator for straight tunnels with rectangular cross section. Key holes effect in tunnel has also been briefly presented.

9.5 General conclusion regarding state of the art related to Channel models for Railway environments

The characterization of the channel models for railway environments is a large topic due to the diversity of common environments that a train can encounter during a ride. We have considered channel models obtained with measurements and simulations along high speed lines and tunnels. We identified several channel models that can be used in Emulradio4Rail platform for T2G communications along HSL. The choice remains limited because (a) we need to have TDL, eventually CDL, models and (b) the number of works dealing with such models is limited. Moreover we did not find a suitable model for the tunnel case and further measurement campaigns and data analysis are needed to derive such models.

The chosen models will prove the feasibility of a real-time evaluation of the radio link inside the complete platform. Extension will be necessary to improve the capabilities of the plateform: either developping new TDL models for the missing cases or including more complex emulation solutions that offer higher accuracy but at the cost of complexity.

10 Applicability analysis of the channel models for the emulation platform

10.1 Introduction

In this applicability analysis we include a description of the methodology to identify the most suitable channel models and also the summary of the proposed models to be implemented in the platform. An exhaustive survey of the state-of-the-art of radio channel models in railways has been done based on literature study during the project and was presented in the previous section. The outcome is that there are different channel models in the literature but not all of them seem to be suitable to be implemented in channel emulator and, more specific, to provide a complete description of the channel. In particular, a description of the Doppler spectrum is missing many times.

The emulation needs to be performed under specific conditions, in order to address on an efficient way, the scenarios, services, perturbations and technologies that have been requested. On the other hand, there are some constraints that come from the available technology for the emulation platform. In particular, the channel emulator only accepts tapped-delay line (TDL) channel models, therefore, all the selected channels must be TDL-based. Moreover, there is a limitation in the number of taps that the emulator is able to handle, so we can't accept all the TDL-based channels as they are.

10.2 Methodology

Regarding the completeness of the channel information, models should include the following information of the channel:

- Number of taps.
- Delay associated to each tap.
- Relative power associated to each tap (relative to the 1st one).
- Speed range considered.
- Doppler spectrum (i.e. distribution of the frequency shift in the Doppler domain).
- Frequency range.
- Bandwidth considered.
- Diversity (*i.e.* SISO, MIMO, *etc.*).

Consequently, the approach is to choose the TDL-based model that provides a more detailed description of the channel in each scenario. In case we have many of them that fulfill this condition, we will choose the one that is based on similar premises as we are (*i.e.* frequency bands close to those related to LTE and IEEE 802.11, bandwidth and vehicular speed).

In particular, LTE emulation will be focused on both 900 MHz and 1.9 GHz and IEEE 802.11 (Wi-Fi) will be focused on 2.4 GHz. Therefore, in case of doubt we prefer to have channels models whose frequencies are closer to our bands of interest.

Finally, channel models based on measurements are preferable to models based on simulations only.

10.3 Summary of the channel models most suitable for emulation

In this section we summarize the channels we have found more suitable to be emulated with the premises we have explained before. In table 16 a summary is provided.

Scenario	Model	Comments
Hilly	[123]	ETSI 6 taps model at 900 MHz and 100 km/h
Rural	[12]	
Viaduct	[5]	Frequency band of the model (2.35 GHz) is not close to the bands of interest for this scenario
Cutting	[6]	
Tunnel	[8]	Provided model is a Winner model not easy to emulate

Table 16: The selected models

10.3.1 Hilly Terrain

In this scenario two models are identified. First, we consider the SISO model described in the ETSI document [123]. This model is based on measurements in the 900 MHz band at a speed of 100 km/h. MIMO setups were not considered and information on Doppler spectrum is available (the classical one, which is also called Jakes' Spectrum). The considered bandwidth is up to 5 MHz. Both the time reference and the associated power for each tap is shown in table 17. The ETSI document present several models with 12 taps and a reduced version with 6 taps. For each model two equivalent alternative tap settings, indicated respectively by (1) and (2) in the appropriate columns, are given. We have chosen the 6 taps model as a first proof of concept but depending on the emulator capabilities, an extension to 12 taps is feasible.
Second, another potential TDL-based model for hilly terrain can be considered [11] for SISO configuration. It provides the same information as [123] (including Doppler spectrum) and it is given in table 12. It was measured at a higher speed but it is based on 2.6 GHz, which made it an interesting option for emulation of IEEE 802.11 at 2.4 GHz. The problem is that in hilly scenarios it is very unlikely that the train-to-ground communications will be based on IEEE 802.11 systems (which is more likely for urban, depots, stations and subway tunnels, but not for regional or high-speed trains).

Tap number	Relative time (μs)		Relative power (dB)	
1	(1) 0.0	(2) 0.0	(1) 0.0	(2) 0.0
2	0.1	0.2	-1.5	-2.0
3	0.3	0.4	-4.5	-4.0
4	0.5	0.6	-7.5	-7.0
5	15.0	15.0	-8.0	-6.0
6	17.2	17.2	-17.7	-12.0

Table 17: Selected model for Hilly terrain extracted from ETSI report in the 900 MHz band [17]

10.3.2 Rural scenario

The model is extracted from [12]. It was obtained thanks to measurements in the 2.4 GHz band in the environment illustrated on figure 21. The TDL parameters are given in the following table 18. The Doppler spectrum considered for each tap is the Jakes model or Classical model. The other TDL model that could be considered, is the GSM rural area standard model from [123] given in table given figure 20. Another model is extracted from [9]. Table 19 summarizes the information.

10.3.3 Viaduct

In viaducts one TDL channel model was found in [5]. This model is based on measurements taken at 2.35 GHz which is far away from the LTE bands of interest for the Emulradio4Rail project. The Doppler spectrum follows a discrete distribution with three possible values for the Doppler shift depending on

Figure 21: Rural environment for HSL in China [9]

Parameter	Value		
Center frequency	2.4 GHz		
Bandwidth	5 MHz		
Speed	240 km/h		
Antenna configuration	SISO		
Scenario	Tap	Delay (μs)	Relative power (dB)
Rural	1	0	0
	2	0.3	-12.9
	3	0.6	-22.9

Table 18: TDL characteristics of rural HSL model obtained in [12]

the region (far or not from the transmitting point) and also on the tap. In table 6 relative power and time for each tap and Doppler shift are shown. The other parameters for this model are a bandwidth of 10 MHz, SISO-only and measurements were taken at 240 km/h.

10.3.4 Cutting

In the cutting scenario we found three different models: [6], [66], [12]. The three of them are measured at high speeds, neither of them consider MIMO schemes and all of them provide information about the Doppler spectrum. Regarding the frequency band they differ, because [6] covers both 950 MHz and 2.15 GHz; [66] covers 2.35 GHz and [12] 2.4 GHz. For this reason, we chose [6]. The TDL parameters for this model are shown in table 10 and the Doppler shift is bounded between 100 and 260 Hz at 950 MHz, and 200-600 Hz at 2.15 GHz. The vehicle speed was 310 km/h and the bandwidth is 20 MHz.

10.3.5 Tunnel scenario

It is noteworthy to say that in the scientific literature there is no TDL-based model for tunnels. This could be due to many different reasons, one of them the high temporal resolution that is needed to be achieved in order to obtain the multipath components that may exist on a tunnel.

Considering existing tools for deterministic simulation of the radio channel as a possibility in this new version of this deliverable we include a TDL model based on ray-tracing simulations carried out Ray-Tracer developed by the Beijing Jiaotong University in China [124].

Given that subway and high-speed tunnels differ in many aspects and also that the operational aspects are not equal (*i.e.* train speed, tunnel size, *etc.*), we provide a twofold TDL channel model: one for a high-speed tunnel and the other one for a subway tunnel.

In Tables 21, 22, 23, and 24, the 2x2 MIMO TDL model for the HSR tunnel is depicted. In these four tables we can see both the power and delay figures related to each of the 11 taps which comprise each one of the subchannels of the 2x2 MIMO channel (h_{11}, h_{12}, h_{21} and h_{22}). Due to the simulation limitation (delay was lower-bounded to 8 ns) the number of MPCs we are able to identify is limited.

Parameter	Value		
Center frequency	1.85 GHz		
Bandwidth	20 MHz		
Speed	0-300 km/h		
Antenna configuration	SISO		
Scenario	Tap	Delay (ns)	Relative power (dB)
Rural	1	0.2	0
	2	1.2	-14.5

Table 19: TDL characteristics for Hilly terrain extracted from [9]

Tap number	Relative time (μ s)		Relative power (dB)		Doppler spectrum
	(1)	(2)	(1)	(2)	
1	0.0	0.0	0.0	0.0	RICE
2	0.1	0.2	-4.0	-2.0	CLASS
3	0.2	0.4	-8.0	-10.0	CLASS
4	0.3	0.6	-12.0	-20.0	CLASS
5	0.4		-16.0		CLASS
6	0.5		-20.0		CLASS

Table 20: GSM rural model with 6 taps in [17]

In order to identify multipath components (MPCs) the power threshold is set at $30\ dB$ below the maximum tap.

The best fit for the fading distribution is Weibull and the values of the distribution parameters for each tap are provided as well in Tables 21-24. The Weibull distribution follows this expression:

$$\mathrm{pdf}(|\alpha|;\beta_w,\Omega_{\mathrm{weib}}) = \frac{\beta_w}{\Omega_{\mathrm{weib}}}|\alpha|^{\beta_w-1}\cdot e^{(-\frac{|\alpha|^{\beta_w}}{\Omega_{\mathrm{weib}}})} \tag{22}$$

In this scenario, the speed for the train is 350 km/h, and the carrier frequency is 2.4 GHz which means a maximum Doppler shift of ±800 Hz. Regarding the Doppler spectrum, all the taps in the models are Jakes' shaped and the distribution which fits better the Jakes' σ related to the model is log-logistic (see tables 21-24).

In subway tunnels the simulations are the same as for HSR tunnels but on a shorter tunnel, trains run slower (up to 110 km/h) and trains are smaller as well. In subway tunnels we have 5 solvable multipath components instead of 11 as in HSR.

Tap No.	Path Power		Fading Distribution		Doppler Spectrum			
	(lin.)	(dB)	Weibull		Shape	Fitting Model of σ_{Jakes}	μ_{LL}	σ_{LL}
			β_ω	Ω_{weib}				
1	1	0	0.17	0.69	Jakes	Log-Logistic	0.0232	0.2397
2	0.2550	-5.9354	0.69	0.38	Jakes	Log-Logistic	-1.1955	0.2263
3	0.1645	-7.8387	0.52	0.35	Jakes	Log-Logistic	-1.1289	0.1863
4	0.1242	-9.0596	0.36	0.44	Jakes	Log-Logistic	-0.9383	0.2453
5	0.0472	-13.2576	0.48	0.78	Jakes	Log-Logistic	-0.7976	0.3371
6	0.0313	-15.0394	0.59	1.00	Jakes	Log-Logistic	-0.6182	0.2581
7	0.0129	-18.8940	0.48	0.94	Jakes	Log-Logistic	-0.6448	0.1544
8	0.0266	-16.8539	0.56	1.04	Jakes	Log-Logistic	-0.5082	0.1022
9	0.0140	-18.5330	0.62	1.36	Jakes	None	σ_{Jakes}	
							0.4654	
10	0.0033	-24.8490	0.92	2.78	Jakes	None	0.4081	
11	0.0017	-27.7257	0.88	3.35	Jakes	None	0.4435	

Table 21: TDL parameters of h_{11} for HSR tunnel scenario

Tap No.	Path Power		Fading Distribution		Doppler Spectrum			
	(lin.)	(dB)	Weibull		Shape	Fitting Model of σ_{Jakes}	μ_{LL}	σ_{LL}
			β_ω	Ω_{weib}				
1	1	0	1.17	0.69	Jakes	Log-Logistic	0.0232	0.2397
2	0.2563	-5.9125	0.69	0.38	Jakes	Log-Logistic	-1.1955	0.2269
3	0.1654	-7.8156	0.52	0.35	Jakes	Log-Logistic	-1.2885	0.1851
4	0.1240	-9.0657	0.36	0.44	Jakes	Log-Logistic	-0.9382	0.2452
5	0.0464	-13.3303	0.48	0.78	Jakes	Log-Logistic	-0.7983	0.3357
6	0.0314	-15.0252	0.59	1.01	Jakes	Log-Logistic	-0.6083	0.2638
7	0.0123	-19.0947	0.50	0.94	Jakes	Log-Logistic	-0.6447	0.1537
8	0.0207	-16.8403	0.56	1.03	Jakes	Log-Logistic	-0.5084	0.1045
9	0.0134	-18.7221	0.60	1.27	Jakes	None	σ_{Jakes}	
							0.4538	
10	0.0039	-24.1345	0.90	2.76	Jakes	None	0.4194	
11	0.0017	-27.8016	0.86	3.17	Jakes	None	0.4434	

Table 22: TDL parameters of h_{12} for HSR tunnel scenario

Tap No.	Path Power		Fading Distribution		Doppler Spectrum			
	(lin.)	(dB)	Weibull		Shape	Fitting Model of σ_{Jakes}	μ_{LL}	σ_{LL}
			β_ω	Ω_{weib}				
1	1	0	1.15	0.68	Jakes	Log-Logistic	0.0333	0.2369
2	0.2556	-5.9253	0.70	0.37	Jakes	Log-Logistic	-1.1919	0.2252
3	0.1440	-8.4177	0.53	0.36	Jakes	Log-Logistic	-1.2911	0.1878
4	0.1229	-9.1056	0.36	0.43	Jakes	Log-Logistic	-0.9459	0.2436
5	0.0497	-13.0347	0.49	0.81	Jakes	Log-Logistic	-0.7684	0.3655
6	0.0363	-14.3972	0.57	1.02	Jakes	Log-Logistic	-0.6153	0.2563
7	0.0132	-18.8071	0.49	0.89	Jakes	Log-Logistic	-0.6381	0.1596
8	0.0070	-21.5761	0.65	1.38	Jakes	Log-Logistic	-0.5238	0.1158
9	0.0149	-18.2809	0.59	1.35	Jakes	None	σ_{Jakes}	
							0.4530	
10	0.0039	-24.0510	0.89	2.70	Jakes	None	0.4189	
11	0.0017	-27.7583	0.85	2.91	Jakes	None	0.4419	

Table 23: TDL parameters of h_{21} for HSR tunnel scenario

Tap No.	Path Power		Fading Distribution		Doppler Spectrum			
	(lin.)	(dB)	Weibull		Shape	Fitting Model of σ_{Jakes}	μ_{LL}	σ_{LL}
			β_ω	Ω_{weib}				
1	1	0	1.15	0.68	Jakes	Log-Logistic	0.0333	0.2368
2	0.2551	-5.9331	0.70	0.37	Jakes	Log-Logistic	-1.1915	0.2258
3	0.1472	-8.3209	0.53	0.35	Jakes	Log-Logistic	-1.2905	0.1863
4	0.1227	-9.1117	0.36	0.43	Jakes	Log-Logistic	-0.9459	0.2435
5	0.0498	-13.0290	0.49	0.81	Jakes	Log-Logistic	-0.7689	0.3655
6	0.0365	-14.3812	0.57	1.03	Jakes	Log-Logistic	-0.6076	0.2609
7	0.0129	-18.8986	0.49	0.86	Jakes	Log-Logistic	-0.6396	0.1604
8	0.0071	-21.4619	0.65	1.37	Jakes	Log-Logistic	-0.5239	0.1157
9	0.0149	-18.2646	0.59	1.35	Jakes	None	σ_{Jakes}	
							0.4533	
10	0.0039	-24.0733	0.89	2.70	Jakes	None	0.4189	
11	0.0016	-27.8333	0.84	2.79	Jakes	None	0.4417	

Table 24: TDL parameters of h_{22} for HSR tunnel scenario

The best fit for the fading distribution is Weibull as in HSR and for the Doppler spectrum the situation is a little different because for the first two taps the best fit is a Burr distribution. For the other three taps, there is no enough solvable data points to estimate the statistical parameters properly. Burr distribution is shown in (23).

$$\text{pdf}(\sigma(s,l);\alpha,c,k) = \frac{\frac{k\cdot c}{\alpha}(\frac{\sigma(s,l)}{\alpha})^{c-1}}{(1+(\frac{\sigma(s,l)}{\alpha})^{c})^{k+1}}, \quad \alpha>0, c>0, k>0 \tag{23}$$

where α is the scale parameter, and c, k are both the shape factors. In Tables 25-28 we provide all the parameters related to this MIMO 2x2 TDL model.

More details on this model are available in [125].

Tap No.	Path Power		Fading Distribution		Doppler Spectrum				
	(lin.)	(dB)	Weibull		Shape	Fitting Model of σ_{Jakes}	α	c	k
			β_ω	Ω_{weib}					
1	1	0	1.22	0.69	Jakes	Burr	0.6119	28.6175	0.2131
2	0.0377	-14.2312	0.68	0.44	Jakes	Burr	0.1568	39.1621	0.1061
3	0.0043	-23.6337	0.50	1.11	Jakes	None	σ_{Jakes}		
							0.1329		
4	0.0070	-21.5570	0.57	1.25	Jakes	None	0.2275		
5	0.0013	-28.9994	0.96	4.02	Jakes	None	0.1991		

Table 25: TDL parameters of h_{11} for subway tunnel scenario

Tap No.	Path Power		Fading Distribution		Doppler Spectrum				
	(lin.)	(dB)	Weibull		Shape	Fitting Model of σ_{Jakes}	α	c	k
			β_ω	Ω_{weib}					
1	1	0	1.22	0.69	Jakes	Burr	0.6121	28.5526	0.2134
2	0.0378	-14.2202	0.68	0.44	Jakes	Burr	0.1568	40.4683	0.1025
3	0.0043	-23.6271	0.50	1.11	Jakes	None	σ_{Jakes}		
							0.1325		
4	0.0070	-21.5352	0.57	1.25	Jakes	None	0.2275		
5	0.0013	-28.9919	0.96	4.02	Jakes	None	0.1991		

Table 26: TDL parameters of h_{12} for subway tunnel scenario

Tap No.	Path Power		Fading Distribution		Doppler Spectrum				
	(lin.)	(dB)	Weibull		Shape	Fitting Model of σ_{Jakes}	α	c	k
			β_ω	Ω_{weib}					
1	1	0	1.19	0.69	Jakes	Burr	0.6179	19.7439	0.3316
2	0.0373	-14.2777	0.67	0.47	Jakes	Burr	0.1575	40.0865	0.1032
3	0.0045	-23.5007	0.53	1.17	Jakes	None	σ_{Jakes}		
							0.1436		
4	0.0075	-21.2624	0.57	1.26	Jakes	None	0.2165		
5	0.0013	-28.7612	0.96	4.02	Jakes	None	0.1991		

Table 27: TDL parameters of h_{21} for subway tunnel scenario

Tap No.	Path Power		Fading Distribution		Doppler Spectrum				
	(lin.)	(dB)	Weibull		Shape	Fitting Model of σ_{Jakes}	α	c	k
			β_ω	Ω_{weib}					
1	1	0	1.19	0.69	Jakes	Burr	0.6182	19.6848	0.3323
2	0.0318	-14.9759	0.67	0.49	Jakes	Burr	0.1575	40.4733	0.1021
3	0.0045	-23.4983	0.53	1.17	Jakes	None	σ_{Jakes}		
							0.1441		
4	0.0075	-21.2391	0.57	1.27	Jakes	None	0.2171		
5	0.0013	-28.7540	0.96	4.02	Jakes	None	0.1991		

Table 28: TDL parameters of h_{22} for subway tunnel scenario

11 Conclusions

This literature analysis performed within the Task 3.1 of WP1 in the Emulradio4Rail project has allowed the identification of a suitable TDL-based channel model for the following railway-related scenario:

- Hilly
- Rural
- Cutting
- Viaduct

. . . with the remarkable exception of tunnels. Therefore, in this new version of the deliverable we have included a brand new TDL model based on ray-tracing simulations for railway tunnels which was developed for this project and published [125]. Now, all the relevant railway scenarios have a suitable TDL-based channel model to be emulated in the Emulradio4Rail platforms.

During this literature survey, we found models in some representative railway scenarios allowing the validation of the channel emulators in the Emulradio4Rail project and the first results for Experimental assessment of IP impairments expected for D3.2.

This conclusion opens important perspectives and particularly the need for further works on channel modelling, and especially the need for some specific measurement campaigns. Another perspective is the possibility to introduce more sophisticated real-time channel emulators able to operate with geometric channel models as well as Winner model widely considered in the standardization bodies.

References

[1] Andreas F.Molisch. *Wireless communications, Second edition*. Wiley, 2011.

[2] Hideichi Sasaoka. *Wave Summit Course: Mobile communications*. Hideichi Sasaoka ed., 2000.

[3] Fernando Perez Fontan, Veikko Hovinen, M Schonhuber, Roberto Prieto-Cerdeira, J Rivera-Castro, Pavel Valtr, J Kyrolainen, and F Teschl. Characterisation of the satellite-to-indoor propagation channel. pages 105 – 110, 09 2008.

[4] C. X. Wang, A. Ghazal, B. Ai, Y. Liu, and P. Fan. Channel measurements and models for high-speed train communication systems: A survey. *IEEE Communications Surveys Tutorials*, 18(2):974–987, 2016.

[5] L. Liu, C. Tao, J. Qiu, H. Chen, L. Yu, W. Dong, and Y. Yuan. Position-Based Modeling for Wireless Channel on High-Speed Railway under a Viaduct at 2.35 GHz. *IEEE Journal on Selected Areas in Communications*, 30(4):834–845, May 2012.

[6] Jianwen Ding, Lei Zhang, Jingya Yang, Bin Sun, and Jiying Huang. Broadband Wireless Channel in Composite High-Speed Railway Scenario: Measurements, Simulation, and Analysis, 2017.

[7] Yvo de Jong Bultitude and Terhi Rautiainen. IST-4-027756 WINNER II D1. 1.2 V1. 2 WINNER II Channel Models. *EBITG, TUI, UOULU, CU/CRC, NOKIA, Tech. Rep*, 2007.

[8] S. Hairoud, P. Combeau, Y. Pousset, Y. Cocheril, and M. Berbineau. WINNER model for subway tunnel at 5.8 GHz. In *2012 12th International Conference on ITS Telecommunications*, pages 743–747, November 2012.

[9] Bangyan Huang, Dongping Yao, Dan Fei, Lei Xiong, and Hongfeng Qin. Development of LTE-based channel tester for high-speed scenario. In *2017 15th International Conference on ITS Telecommunications (ITST)*, pages 1–5, May 2017.

[10] M. Series. Guidelines for evaluation of radio interface technologies for IMT-Advanced. *Report ITU*, (2135-1), 2009.

[11] W. Qian, X. Chunxiu, Z. Min, and Y. Deshui. Results and analysis for a novel 2 #x00d7;2 channel measurement applied in LTE-R at 2.6 GHz. In *2014 IEEE Wireless Communications and Networking Conference (WCNC)*, pages 177–181, April 2014.

[12] Liu Liu, Cheng Tao, Tao Zhou, Youping Zhao, Xuefeng Yin, and Houjin Chen. A highly efficient channel sounding method based on cellular communications for high-speed railway scenarios. *EURASIP Journal on Wireless Communications and Networking*, 2012(1):307, December 2012.

[13] Yan Zhang, Zunwen He, Wancheng Zhang, Limin Xiao, and Shidong Zhou. Measurement-Based Delay and Doppler Characterizations for High-Speed Railway Hilly Scenario, 2014.

[14] W. Qian, X. Chunxiu, W. Muqing, Z. Min, and Y. Deshui. Propagation characteristics of high speed railway radio channel based on broadband measurements at 2.6 GHz. In *2014 IEEE Wireless Communications and Networking Conference (WCNC)*, pages 166–170, April 2014.

[15] Ist-4-027756 winner ii d1.1.2 v1.0 - winner ii channel models part ii - radio channel measurement and analysis results. Technical report, 2007.

[16] Ist-4-027756 winner ii d1.1.2 v1.2 - winner ii channel models part i - channel models. Technical report, 2007.

[17] *Digital cellular telecommunications system (Phase 2+) (GSM) - GSM/EDGE Background for Radio Frequency (RF) requirements - 3GPP TR 45.050 version 14.0.0 Release 14*. 2017.

[18] R. Torrego, M. Bouaziz, J. Soler, A. Vizzarri, M. Berbineau, and J. Moreno. Deliverable d 2.1: Solutions to emulate the radio bearer (stream b), public, h2020-s2r-oc-ip2-2018-03. 2019.

[19] J. Moreno, M. Berbineau, C. Gransart, A. Vizzari, R. Torrego, J. Soler, and Y. Yan. Deliverable d1.1 - application layer requirements for communications systems in railway environments (stream a), public, h2020-s2r-oc-ip2-2018-03. 2019.

[20] L. Clavier, P. Mariage, S. Karbech, R. Torrego, V. Inaki, A. Arriola, V. Deniau, A. Vizarri, J. Moreno, and R. Kassi. Deliverable d1.2 - present and future railway communications scenarios: description of perturbations with impact on railway communications (stream c), h2020-s2r-oc-ip2-2018-03, public. 2019.

[21] R. Torrego, P. Aljama, M. Berbineau, J. Soler, Y. Yan, L. Clavier, S. Kharbech, and A. Vizzarri. Deliverable d 3.1 - high-level design of radio access emulation tool (stream b), h2020-s2r-oc-ip2-2018-03, public. 2019.

[22] Jean-Marc Kwadjane. *Apport de la connaissance a priori de la position de l'émetteur sur les algorithmes MIMO adaptatifs en environnement tunnel pour les métro*. PhD thesis, PhD thesis, Université de Lille, December 2014.

[23] Gérald Moniak. *Techniques MIMO pour un lien sans fil robuste entre un bus et un poste de contrôle pour une application de surveillance embarquée*. PhD thesis, PhD thesis, L'Université de Valenciennes et du Hainaut Cambresis, February 2007.

[24] A. F. Molisch. A generic model for mimo wireless propagation channels in macro- and microcells. *IEEE Transactions on Signal Processing*, 52(1):61–71, Jan 2004.

[25] J. D. Parsons. *The Mobile Radio Propagation Channel*. Pentech Press, 1992.

[26] J. G. Proakis. *Wireless Communications*. Pearso, 2007.

[27] A. Goldsmith. *Digital Signal Processing, 4th Edition*. Cambridge University Press, 2005.

[28] T. S. Rappaport. *Wireless Communications*. Prentice Hall, 2002.

[29] Ana Aguiar and James Gross. Wireless channel models. 04 2003.

[30] Michel Mfeze and Emmanuel Tonye. Comparative Approach of Doppler Spectra for Fading Channel Modelling by the Filtered White Gaussian Noise Method. *International Journal of Computer Science and Telecommunications*, 6(11):1, 2015.

[31] Philip Bello. Characterization of randomly time-variant linear channels. *IEEE transactions on Communications Systems*, 11(4):360–393, 1963.

[32] Gregory J. Pottie and William J. Kaiser. *Principles of Embedded Networked Systems Design*. Cambridge University Press, 2005.

[33] Philippe Guguen. *Techniques multi-antennes émission-réception ; Applications aux réseaux domestiques sans fil*. PhD thesis, PhD thesis, INSA de Rennes, September 2003.

[34] Robert G. Gallager. *Information Theory and Reliable Communication*. Wiley, 1966.

[35] C.F. Van Loan G.H. Golub. *Matrix computations.* Johns Hopkins university press, 1996.

[36] M. Steinbauer, A. F. Molisch, and E. Bonek. The double-directional radio channel. *IEEE Antennas and Propagation Magazine*, 43(4):51–63, Aug 2001.

[37] Julien Guillet. *Caractérisation et modélisation spatio-temporelles du canal de propagation radioélectrique dans le contexte MIMO*. PhD Thesis, INSA de Rennes, 2004.

[38] P. Bello. Characterization of randomly time-variant linear channels. *IEEE Transactions on Communications Systems*, 11(4):360–393, December 1963.

[39] P. Petrus, J. H. Reed, and T. S. Rappaport. Geometrical-based statistical macrocell channel model for mobile environments. *IEEE Transactions on Communications*, 50(3):495–502, March 2002.

[40] 3gpp tr 25.996 v14.0.0 (2017-03) 3rd generation partnership project technical specification group radio access network spatial channel model for multiple input multiple output (mimo) simulations. Technical report, 2017.

[41] P. Almers, E. Bonek, A. Burr, N. Czink, M. Debbah, V. Degli-Esposti, H. Hofstetter, P. Kyösti, D. Laurenson, G. Matz, A. F. Molisch, C. Oestges, and H. Özcelik. Survey of channel and radio propagation models for wireless mimo systems. *EURASIP J. Wirel. Commun. Netw.*, 2007(1):56–56, January 2007.

[42] D. S. Baum, J. Hansen, and J. Salo. An interim channel model for beyond-3g systems: extending the 3gpp spatial channel model (scm). In *2005 IEEE 61st Vehicular Technology Conference*, volume 5, pages 3132–3136 Vol. 5, May 2005.

[43] wp5: Final report on link level and system level channel models. deliverable d5.4, November 2005.

[44] Juha Meinilä, Pekka Kyösti, Lassi Hentilä, Tommi Jämsä, Essi Suikkanen, Esa Kunnari, and Milan Narandžić. Document Title: D5. 3: WINNER+ Final Channel Models.

[45] Vuokko Nurmela, Aki Karttunen, Antti Roivainen, Leszek Raschkowski, Veikko Hovinen, Juha Ylitalo EB, Nobutaka Omaki, Katsutoshi Kusume, Aki Hekkala, and Richard Weiler. Deliverable d1. 4 METIS channel models. In *Proc. Mobile Wireless Commun. Enablers Inf. Soc.(METIS)*, page 1, 2015.

[46] Itu-r m.1225 - guidelines for evaluation of radio transmission technologies for imt-2000. Technical report, 1997.

[47] M. Gudmundson. Correlation model for shadow fading in mobile radio systems. *Electron. Lett.*, 27,23:2145–2146, 1991.

[48] A. A. M. Saleh and R. Valenzuela. A Statistical Model for Indoor Multipath Propagation. *IEEE Journal on Selected Areas in Communications*, 5(2):128–137, February 1987.

[49] A. Abdi and M. Kaveh. A space-time correlation model for multielement antenna systems in mobile fading channels. *IEEE Journal on Selected Areas in Communications*, 20(3):550–560, April 2002.

[50] Q. H. Spencer, B. D. Jeffs, M. A. Jensen, and A. L. Swindlehurst. Modeling the statistical time and angle of arrival characteristics of an indoor multipath channel. *IEEE Journal on Selected Areas in Communications*, 18(3):347–360, March 2000.

[51] Ke Guan, Zhangdui Zhong, and Bo Ai. Assessment of LTE-R Using High Speed Railway Channel Model. pages 461–464. IEEE, April 2011.

[52] L. Tian, X. Yin, Q. Zuo, J. Zhou, Z. Zhong, and S. X. Lu. Channel modeling based on random propagation graphs for high speed railway scenarios. In *2012 IEEE 23rd International Symposium on Personal, Indoor and Mobile Radio Communications - (PIMRC)*, pages 1746–1750, September 2012.

[53] T. Zhou, C. Tao, S. Salous, L. Liu, and Z. Tan. Channel sounding for high-speed railway communication systems. *IEEE Communications Magazine*, 53(10):70–77, October 2015.

[54] T. Zhou, C. Tao, S. Salous, L. Liu, and Z. Tan. Implementation of an LTE-Based Channel Measurement Method for High-Speed Railway Scenarios. *IEEE Transactions on Instrumentation and Measurement*, 65(1):25–36, January 2016.

[55] Tomás Domínguez-Bolaño, José Rodríguez-Piñeiro, José A. García-Naya, and Luis Castedo. Experimental Characterization of LTE Wireless Links in High-Speed Trains. *Wireless Communications and Mobile Computing*, 2017:1–20, 2017.

[56] Jingya Yang, Bo Ai, Danping He, Longhe Wang, Zhangdui Zhong, and Andrej Hrovat. A Simplified Multipath Component Modeling Approach for High-Speed Train Channel Based on Ray Tracing, 2017.

[57] A. Ghazal, Y. Yuan, C. X. Wang, Y. Zhang, Q. Yao, H. Zhou, and W. Duan. A Non-Stationary IMT-Advanced MIMO Channel Model for High-Mobility Wireless Communication Systems. *IEEE Transactions on Wireless Communications*, 16(4):2057–2068, April 2017.

[58] J. Bian, J. Sun, C. X. Wang, R. Feng, J. Huang, Y. Yang, and M. Zhang. A WINNER #x002b; Based 3-D Non-Stationary Wideband MIMO Channel Model. *IEEE Transactions on Wireless Communications*, 17(3):1755–1767, March 2018.

[59] R. He, Z. Zhong, B. Ai, G. Wang, J. Ding, and A. F. Molisch. Measurements and Analysis of Propagation Channels in High-Speed Railway Viaducts. *IEEE Transactions on Wireless Communications*, 12(2):794–805, February 2013.

[60] K. Guan, Z. Zhong, B. Ai, and T. Kurner. Deterministic Propagation Modeling for the Realistic High-Speed Railway Environment. In *2013 IEEE 77th Vehicular Technology Conference (VTC Spring)*, pages 1–5, June 2013.

[61] Rongchen Sun, Cheng Tao, Liu Liu, Zhenhui Tan, Lingwen Zhang, and Tao Zhou. Nonisotropic Scattering Characteristic in an Alternant Tree-Blocked Viaduct Scenario on High-Speed Railway at 2.35 GHz, 2014.

[62] D. He, J. Yang, K. Guan, B. Ai, Z. Zhong, Z. Zhao, D. Miao, and H. Guan. Ray-tracing simulation and analysis of propagation for 3gpp high speed scenarios. In *2017 11th European Conference on Antennas and Propagation (EUCAP)*, pages 2890–2894, March 2017.

[63] T. Zhou, C. Tao, S. Salous, and L. Liu. Measurements and Analysis of Angular Characteristics and Spatial Correlation for High-Speed Railway Channels. *IEEE Transactions on Intelligent Transportation Systems*, 19(2):357–367, February 2018.

[64] R. He, Z. Zhong, B. Ai, J. Ding, Y. Yang, and A. F. Molisch. Short-Term Fading Behavior in High-Speed Railway Cutting Scenario: Measurements, Analysis, and Statistical Models. *IEEE Transactions on Antennas and Propagation*, 61(4):2209–2222, April 2013.

[65] L. Tian, J. Zhang, and C. Pan. Small Scale Fading Characteristics of Wideband Radio Channel in the U-Shape Cutting of High-Speed Railway. In *2013 IEEE 78th Vehicular Technology Conference (VTC Fall)*, pages 1–6, September 2013.

[66] R. Sun, C. Tao, L. Liu, and Z. Tan. Channel Measurement and Characterization for HSR U-Shape Groove Scenarios at 2.35 GHz. In *2013 IEEE 78th Vehicular Technology Conference (VTC Fall)*, pages 1–5, September 2013.

[67] K. Guan, Z. Zhong, B. Ai, and T. Kürner. Propagation Measurements and Analysis for Train Stations of High-Speed Railway at 930 MHz. *IEEE Transactions on Vehicular Technology*, 63(8):3499–3516, October 2014.

[68] Y. Zhang, Y. Liu, J. Sun, C. X. Wang, and X. Ge. Impact of Different Parameters on Channel Characteristics in a High-Speed Train Ray Tracing Tunnel Channel Model. In *2017 IEEE 85th Vehicular Technology Conference (VTC Spring)*, pages 1–5, June 2017.

[69] K. Guan, B. Ai, Z. Zhong, C. F. López, L. Zhang, C. Briso-Rodríguez, A. Hrovat, B. Zhang, R. He, and T. Tang. Measurements and Analysis of Large-Scale Fading Characteristics in Curved Subway Tunnels at 920 MHz, 2400 MHz, and 5705 MHz. *IEEE Transactions on Intelligent Transportation Systems*, 16(5):2393–2405, October 2015.

[70] J. Li, Y. Zhao, J. Zhang, R. Jiang, C. Tao, and Z. Tan. Radio channel measurements and analysis at 2.4/5ghz in subway tunnels. *China Communications*, 12(1):36–45, January 2015.

[71] C. Gentile, F. Valoit, and N. Moayeri. A raytracing model for wireless propagation in tunnels with varying cross section. In *2012 IEEE Global Communications Conference (GLOBECOM)*, pages 5027–5032, December 2012.

[72] K. Guan, Z. Zhong, B. Ai, R. He, B. Chen, Y. Li, and C. Briso-Rodríguez. Complete Propagation Model in Tunnels. *IEEE Antennas and Wireless Propagation Letters*, 12:741–744, 2013.

[73] L. Zhang, C. Briso, J. R. O. Fernandez, J. I. Alonso, C. Rodríguez, J. M. García-Loygorri, and K. Guan. Delay Spread and Electromagnetic Reverberation in Subway Tunnels and Stations. *IEEE Antennas and Wireless Propagation Letters*, 15:585–588, 2016.

[74] Concepcion Garcia-Pardo, Jose-Maria Molina-García-Pardo, Martine Lienard, Davy P. Gaillot, and Pierre Degauque. Double directional channel measurements in an arched tunnel and interpretation using ray tracing in a rectangular tunnel. *Progress In Electromagnetics Research*, 22:91–107, 2012.

[75] K. Guan, Z. Zhong, J. I. Alonso, and C. Briso-Rodriguez. Measurement of Distributed Antenna Systems at 2.4 GHz in a Realistic Subway Tunnel Environment. *IEEE Transactions on Vehicular Technology*, 61(2):834–837, February 2012.

[76] K. Guan, Z. Zhong, B. Ai, and C. Briso-Rodriguez. Propagation mechanism modelling in the near region of circular tunnels. *Antennas Propagation IET Microwaves*, 6(3):355–360, February 2012.

[77] K. Guan, X. Lin, D. He, B. Ai, Z. Zhong, Z. Zhao, D. Miao, H. Guan, and T. Kürner. Scenario modules and ray-tracing simulations of millimeter wave and terahertz channels for smart rail mobility. In *2017 11th European Conference on Antennas and Propagation (EUCAP)*, pages 113–117, March 2017.

[78] X. Ye, X. Cai, H. Wang, and X. Yin. Tunnel and Non-Tunnel Channel Characterization for High-Speed-Train Scenarios in LTE-A Networks. In *2016 IEEE 83rd Vehicular Technology Conference (VTC Spring)*, pages 1–5, May 2016.

[79] H. d Zheng and X. y Nie. GBSB Model for MIMO Channel and Its Space-Time Correlataion Analysis in Tunnel. In *2009 International Conference on Networks Security, Wireless Communications and Trusted Computing*, volume 1, pages 8–11, April 2009.

[80] Y. Jia, M. Zhao, W. Zhou, and D. Peng. Measurement and statistical analysis of 1.89ghz radio propagation in a realistic mountain tunnel. In *2015 International Conference on Wireless Communications Signal Processing (WCSP)*, pages 1–5, October 2015.

[81] D. J. Cichon, T. C. Becker, and W. Wiesbeck. Determination of time-variant radio links in high-speed train tunnels by ray optical modeling. In *IEEE Antennas and Propagation Society International Symposium. 1995 Digest*, volume 1, pages 508–511 vol.1, June 1995.

[82] X. Cai, X. Yin, X. Cheng, and A. Pérez Yuste. An Empirical Random-Cluster Model for Subway Channels Based on Passive Measurements in UMTS. *IEEE Transactions on Communications*, 64(8):3563–3575, August 2016.

[83] Xiao Chen, Yuntian Pan, Yiming Wu, and Guoxin Zheng. Research on Doppler spread of multipath channel in subway tunnel. In *2014 IEEE International Conference on Communiction Problem-solving*, pages 56–59, December 2014.

[84] C. Briso-Rodriguez, J. M. Cruz, and J. I. Alonso. Measurements and Modeling of Distributed Antenna Systems in Railway Tunnels. *IEEE Transactions on Vehicular Technology*, 56(5):2870–2879, September 2007.

[85] E. Masson, Y. Cocheril, M. Berbineau, J. P. Ghys, J. Kyrolainen, and V. Hovinen. 4 #x00d7;4 MIMO channel sounding in tunnels for train-to-wayside communications. In *2012 International Conference on Wireless Communications in Underground and Confined Areas*, pages 1–5, August 2012.

[86] L. Zhang, J. R. Fernandez, C. B. Rodríguez, C. Rodríguez, J. Moreno, and K. Guan. Broadband radio communications in subway stations and tunnels. In *2015 9th European Conference on Antennas and Propagation (EuCAP)*, pages 1–5, May 2015.

[87] Danping He, Bo Ai, Ke Guan, Zhangdui Zhong, Bing Hui, Junhyeong Kim, Heesang Chung, and Ilgyu Kim. Stochastic Channel Modeling for Railway Tunnel Scenarios at 25 GHz. *ETRI Journal*, 40(1):39–50, February 2018.

[88] R. He, Z. Zhong, B. Ai, K. Guan, B. Chen, J. I. Aionso, and C. Briso. Propagation channel measurements and analysis at 2.4 GHz in subway tunnels. *Antennas Propagation IET Microwaves*, 7(11):934–941, August 2013.

[89] Yann Cocheril, Marion Berbineau, Pierre Combeau, and Yannis Pousset. On the Importance of the MIMO Channel Correlation in Underground Railway Tunnels. *Journal of Communication*, 4(4):224–231, May 2009.

[90] ”sencity rail antenna: 1399.17.0039 huber+suhner data sheet,” huber+suhner ag rf industrial. Technical report, 2010.

[91] Yu Liu, Ammar Ghazal, Cheng-Xiang Wang, Xiaohu Ge, Yang Yang, and Yapei Zhang. Channel measurements and models for high-speed train wireless communication systems in tunnel scenarios: a survey. *Science China Information Sciences*, 60(10):101301, October 2017.

[92] Yan Zhang, Ove Edfors, Peter Hammarberg, Tommy Hult, Xiang Chen, Shidong Zhou, Limin Xiao, and Jing Wang. A general coupling-based model framework for wideband mimo channels. *IEEE Transactions on Antennas and Propagation*, 60(2):574–586, 2012.

[93] A. G. Emslie and R. L. Lagace. Theory of the Propagation of UHF Radio Waves in Coal Mine Tunnels. *IEEE-ANT*, 23(2):192–205, March 1975.

[94] Jorge Avella Castiblanco. *Electromagnetic modeling for antenna design and specifications in tunnels of arbitrary cross-section and answering to the electromagnetic constraints of the environment of the railway domain*. Lille 1, April 2013.

[95] H. Chang, Y. Wu, S. Lu, W. Cheng, and M. Sheng. Field analysis of dielectric waveguide devices based on coupled transverse-mode integral equation-numerical investigation. *Progress In Electromagnetics Research*, 97:159–176, 2009.

[96] SY. Reutskiy. The methods of external excitation for analysis of arbitrarily-shaped hollow conducting waveguides. *Progress In Electromagnetics Research*, 82:203–226, 2008.

[97] A. V. Popov and Ning Yan Zhu. Modeling radio wave propagation in tunnels with a vectorial parabolic equation. *IEEE-ANT*, 48(9):1403–1412, Sep 2000.

[98] S. F. Mahmoud. Characteristics of Electromagnetic Guided Waves for Communication in Coal Mine Tunnels. *IEEE-COM*, 22:1547–1554, October 1974.

[99] M. Agunaou, S. Belattar, P. Mariage, and P. Degauque. Propagation d'ondes électromagnétiques hyperfréquences à l'intérieur d'un métro - Modélisation numérique de l'influence des changements de section. *Revue Transports et Sécurité*, 64:55–68, 1998.

[100] K. Guan, B. Ai, R. He, Z. Zhong, T. Xu, C. Briso-Rodriguez, and A. Hrovat. Stochastic Modeling for Extra Propagation Loss of Tunnel Curve. In *2016 IEEE 83rd Vehicular Technology Conference (VTC Spring)*, pages 1–5, May 2016.

[101] E. Masson. *étude de la propagation des ondes électromagnétiques dans les tunnels courbes de section non droite pour des applications métro et ferroviaire*. PhD thesis, Université de Poitiers, Décembre 2010.

[102] K. D. Laakman and W. H. Steier. Waveguides: characteristic modes of hollow rectangular dielectric waveguides. *Applied Optics*, 15(5):1334–1340, May 1976.

[103] D. G. Dudley and S. F. Mahmoud. Linear source in a circular tunnel. *IEEE Transactions on Antennas and Propagation*, 54(7):2034–2047, July 2006.

[104] D. G. Dudley, S. F. Mahmoud, M. Lienard, and P. Degauque. On wireless communication in tunnels. In *2007 IEEE Antennas and Propagation Society International Symposium*, pages 3305–3308, June 2007.

[105] Jorge Avella Castiblanco. *Electromagnetic Modeling for Antenna design and Specifications in tunnels of any shape answering to the electromagnetic constraints of the environment of the railway domain*. PhD thesis, University of Lille, April 2013.

[106] M. Lienard, P. Degauque, J. Baudet, and D. Degardin. Investigation on MIMO channels in subway tunnels. *IEEE Journal on Selected Areas in Communications*, 21(3):332–339, April 2003.

[107] J. M. Molina-Garcia-Pardo, M. Lienard, A. Nasr, and P. Degauque. Wideband analysis of large scale and small scale fading in tunnels. In *2008 8th International Conference on ITS Telecommunications*, pages 270–273, October 2008.

[108] E. Masson, Y. Cocheril, M. Berbineau, J.P. Ghys, V. Hovinen, and A. Roivanen. Mimo channel characterization in subway tunnel for train-to-wayside applications. *IEEE ITST Proceedings- International Conference in Intelligent Transportation Systems-Telecommunications, Taipei, Taiwan*, pages 732–736, November 2012.

[109] M. Lienard, P. Degauque, J. Baudet, and D. Degardin. Investigation on MIMO channels in subway tunnels. *IEEE-SAC*, 21(3):332–339, Apr 2003.

[110] J. M. Molina-Garcia-Pardo, M. Lienard, P. Degauque, C. Garcia-Pardo, and L. Juan-Llacer. Mimo channel capacity with polarization diversity in arched tunnels. *IEEE Antennas and Wireless Propagation Letters*, 8:1186–1189, 2009.

[111] J. A. Castiblanco, D. Seetharamdoo, M. Berbineau, M. Ney, and F. Gallee. Determination of antenna specification and positioning for efficient railway communication in tunnels of arbitrary cross section. In *ITS Telecommunications (ITST), 2011 11th International Conference on*, pages 678–683, Aug 2011.

[112] A. E. Forooshani, R. D. White, and D. G. Michelson. Effect of antenna array properties on multiple-input-multiple-output system performance in an underground mine. *IET Microwaves, Antennas Propagation*, 7(13):1035–1044, October 2013.

[113] A. E. Forooshani, A. A. Lotfi-Neyestanak, and D. G. Michelson. Optimization of antenna placement in distributed MIMO systems for underground mines. *IEEE-WCOM*, 13(9):4685–4692, Sept 2014.

[114] A. E. Forooshani, C. Y. T. Lee, and D. G. Michelson. Effect of antenna configuration on MIMO-based access points in a short tunnel with infrastructure. *IEEE-COM*, 64(5):1942–1951, May 2016.

[115] David Gesbert, Helmut Bölcskei, Dhananjay Gore, and Arogyaswami Paulraj. Mimo wireless channels: Capacity and performance prediction. In *Global Telecommunications Conference, 2000. GLOBECOM'00. IEEE*, volume 2, pages 1083–1088. IEEE, 2000.

[116] David Gesbert and Jabran Akhtar. Breaking the barriers of shannon's capacity: An overview of mimo wireless systems. *Signal Processing*, 1(B2):B3, 2002.

[117] J. Moreno, L. de Haro, C. Rodríguez, L. Cuéllar, and J. M. Riera. Keyhole estimation of an MIMO-OFDM train-to-wayside communication system on subway tunnels. *IEEE Antennas and Wireless Propagation Letters*, 14:88–91, 2015.

[118] D. Chizhik, G. J. Foschini, M. J. Gans, and R. A. Valenzuela. Keyholes, correlations, and capacities of multielement transmit and receive antennas. *IEEE-WCOM*, 1(2):361–368, Apr 2002.

[119] P. Almers, F. Tufvesson, and A. F. Molisch. Keyhole effect in MIMO wireless channels: Measurements and theory. *IEEE-WCOM*, 5(12):3596–3604, December 2006.

[120] D. G. Dudley, M. Lienard, S. F. Mahmoud, and P. Degauque. Wireless propagation in tunnels. *IEEE-APM*, 49(2):11–26, April 2007.

[121] Javier Alonso Valdesueiro, Benjamin Izquierdo, and Jordi Romeu. On 2x2 mimo observable capacity in subway tunnels at-band: An experimental approach. *Antennas and Wireless Propagation Letters, IEEE*, 9:1099–1102, 2010.

[122] Concepcion Sanchis-Borras, Jose-Maria Molina-Garcia-Pardo, Martine Lienard, and Pierre Degauque. Performance evaluation of mimo-ofdm in tunnels. *Antennas and Wireless Propagation Letters, IEEE*, 11:301–304, 2012.

[123] Etsi 145 005 v13.3.0, digital cellular telecommunications system (phase 2+) (gsm) gsm/edge radio transmission and reception, (3gpp ts 45.0145 005 v13.3.0, release 13). 2017.

[124] D. He, B. Ai, K. Guan, L. Wang, Z. Zhong, and T. Kürner. The design and applications of high-performance ray-tracing simulation platform for 5g and beyond wireless communications: A tutorial. *IEEE Communications Surveys Tutorials*, 21(1):10–27, 2019.

[125] H. Qiu, J. M. Garcia-Loygorri, K. Guan, D. He, Z. Xu, B. Ai, and M. Berbineau. Emulation of radio technologies for railways: a tapped-delay-line channel model for tunnels. *IEEE ACCESS*, pages 1–12, 2020.